



1 **Update a biogeochemical model with process-based**  
2 **algorithms to predict ammonia volatilization from**  
3 **fertilized uplands and rice paddy fields**

4 Siqi Li<sup>1</sup>, Wei Zhang<sup>1</sup>, Xunhua Zheng<sup>1, 2</sup>, Yong Li<sup>1</sup>, Shenghui Han<sup>1</sup>, Rui Wang<sup>1</sup>, Kai  
5 Wang<sup>1</sup>, Zhisheng Yao<sup>1</sup>, Chunyan Liu<sup>1</sup>, Chong Zhang<sup>3</sup>

6 <sup>1</sup>State Key Laboratory of Atmospheric Boundary Layer Physics and Atmospheric Chemistry, Institute of  
7 Atmospheric Physics, Chinese Academy of Sciences, Beijing 100029, P. R. China

8 <sup>2</sup>College of Earth and Planetary Science, University of Chinese Academy of Sciences, Beijing 100049,  
9 P.R. China

10 <sup>3</sup>College of Tropical Crops, Hainan University, Haikou 570228, China

11 *Correspondence to:* Xunhua Zheng (xunhua.zheng@post.iap.ac.cn)

12 Yong Li (yli@mail.iap.ac.cn)

13 **Abstract.** Accurate simulation of ammonia (NH<sub>3</sub>) volatilization from fertilized croplands is crucial to  
14 enhancing fertilizer-use efficiency and alleviating environmental pollution. In this study, a  
15 process-oriented model, CNMM-DNDC (Catchment Nutrient Management Model -  
16 DeNitrification-DeComposition), was evaluated and modified using NH<sub>3</sub> volatilization observations  
17 from 44 and 19 fertilizer application events in cultivated upland areas and paddy rice fields in China,  
18 respectively. The original CNMM-DNDC model not only performed poorly in simulating NH<sub>3</sub>  
19 volatilization from upland areas but also failed to simulate NH<sub>3</sub> volatilization from paddy rice fields. In  
20 the modified CNMM-DNDC model, the major modifications for simulating NH<sub>3</sub> volatilization from  
21 uplands were primarily derived from a peer-reviewed and published study. NH<sub>3</sub> volatilization from  
22 uplands was jointly regulated by the factors of wind speed, soil depth, clay fraction, soil temperature,  
23 soil moisture, vegetation canopy, and rainfall-induced canopy wetting. Moreover, three principle  
24 modifications were made to simulate NH<sub>3</sub> volatilization from paddy rice fields. First, the simulation of  
25 the floodwater layer and its pH were added. Second, the effect of algal growth on the diurnal  
26 fluctuation of floodwater pH was introduced. Finally, the Jayaweera-Mikkelsen model was introduced  
27 to simulate NH<sub>3</sub> volatilization. The modified model showed remarkable performances in simulating the  
28 cumulative NH<sub>3</sub> volatilization of the calibrated and validated cases, with drastically significant  
29 zero-intercept linear regression of slopes of 0.94 ( $R^2 = 0.76$ ,  $n = 40$ ) and 0.98 ( $R^2 = 0.71$ ,  $n = 23$ ),



30 respectively. However, the volatilized  $\text{NH}_3$  simulated by the modified model still exhibited some  
31 deviation from the observations when deep/mixed-placement, irrigation/precipitation, and  
32 prosperous/depressed algal biomass accompanied the fertilizer application events. Future studies still  
33 need to solve these problems to further improve the performance of the modified model. Nevertheless,  
34 the modified model could provide an available method for developing  $\text{NH}_3$  emission inventories and  
35 reducing environmental pollutions.

## 36 **1. Introduction**

37 Synthetic fertilizer application, as the secondary largest contributor to ammonia ( $\text{NH}_3$ ) emissions  
38 after livestock production, accounts for approximately 30% to 50% of anthropogenic  $\text{NH}_3$  emissions  
39 (Behera et al., 2013; Bouwman et al., 1997; Huang et al., 2012; Paulot et al., 2014). The great quantity  
40 of  $\text{NH}_3$  volatilized from agricultural fields contributes to low nitrogen use efficiency for crops (Chien et  
41 al., 2009; Mariano et al., 2019; Zhu et al., 1989). The subsequent dry and wet deposition to terrestrial  
42 ecosystems results in the acidification and eutrophication of natural ecosystems (e.g., Anderson et al.,  
43 2008; Bobbink et al., 1998; Li et al., 2016) and is also considered an indirect source of nitrous oxide  
44 (Martin et al., 2004; Schjørring, 1998). Recently,  $\text{NH}_3$  in the atmosphere has played a vital role in  
45 aerosol formation during several haze periods, which has attracted great attention (e.g., Felix et al.,  
46 2013; Kong et al., 2019; Liu et al., 2018; Savard et al., 2017).

47 Many studies have attempted to estimate ammonia loss from fertilized croplands using  
48 biogeochemical process models, i.e., DeNitrification-DeComposition (DNDC), and water and nitrogen  
49 management (WNMM) (Dubache et al., 2019; Dutta et al., 2016; Giltrap et al., 2017; Michalczyk et al.,  
50 2016; Park et al., 2008). However, these models do not distinguish between the simulation modules of  
51  $\text{NH}_3$  volatilization for uplands and rice paddy fields but rather use the same algorithm (Cannavo et al.,  
52 2008; Li, 2016). It is worth emphasizing that the mechanisms of  $\text{NH}_3$  volatilization are completely  
53 different between fertilized uplands and rice paddy fields due to the presence of floodwater over rice  
54 paddy soils. Recent studies also indicate that estimating  $\text{NH}_3$  emissions without considering rice  
55 cultivation results in large uncertainties (Riddick et al., 2016; Xu et al., 2019). In particular, some  
56 studies have shown that  $\text{NH}_3$  volatilization rates from rice paddy fields are not lower than those of



57 upland crops (Zhou et al., 2016), which also indicates the different mechanisms of  $\text{NH}_3$  volatilization  
58 between fertilized uplands and rice paddy fields. Therefore, using separate modules to simulate  $\text{NH}_3$   
59 volatilization from uplands and rice paddy fields is necessary for the accurate estimation of  $\text{NH}_3$   
60 emissions.

61 Given the totally different mechanisms of  $\text{NH}_3$  volatilization between fertilized uplands and rice  
62 paddy fields, the influencing factors affecting  $\text{NH}_3$  volatilization from uplands are different from those  
63 of rice paddy fields. The dose and application methods of nitrogen fertilizer have been confirmed as the  
64 primary factors affecting  $\text{NH}_3$  volatilization from uplands (e.g., Liu et al., 2003; Roelcke et al., 2002;  
65 Zhang et al., 1992). Moreover, several studies have reported that irrigation and precipitation exert a  
66 complicated influence (stimulated or inhibited) on  $\text{NH}_3$  volatilizations from upland soils (e.g., Han et  
67 al., 2014; Holcomb III et al., 2011; Sanz-Cobena et al., 2011). However, the depth and pH of surface  
68 floodwater, which are unique characteristics of rice paddy fields, were found to be the major factors  
69 influencing  $\text{NH}_3$  volatilization from rice paddy fields (Bowmer and Muirhead, 1987; Hayashi et al.,  
70 2006; Jayaweera and Mikkelsen, 1991). A comprehensive discussion of the influencing factors  
71 affecting  $\text{NH}_3$  volatilization from uplands and rice paddy fields is crucial for providing suggestions to  
72 further improve the performance of process-based biogeochemical models in simulating  $\text{NH}_3$   
73 volatilization from cropland soils and offer specific and pertinent policy advice for the reduction of  
74 ammonia loss.

75 A previous study established a scientific algorithm for the DNDC model to simulate  $\text{NH}_3$   
76 volatilization from fertilized upland soils, which performed well under validation with independent  
77 cases of uplands from China (Li et al., 2019). However, no biogeochemical model has achieved  
78 simulations of  $\text{NH}_3$  volatilization from rice paddy fields using a process-oriented algorithm, although a  
79 classical and extensively used model, i.e., the Jayaweera-Mikkelsen model (J-M model), exists  
80 (Jayaweera and Mikkelsen, 1990a; Li et al., 2008; Wang et al., 2016; Zhan et al., 2019).

81 The Catchment Nutrient Management Model-DeNitrification-DeComposition (CNMM-DNDC)  
82 model, established by coupling the core carbon and nitrogen biogeochemical processes of DNDC (e.g.,  
83 decomposition, nitrification, denitrification and fermentation) into the distributed hydrologic  
84 framework of CNMM, is one of the latest versions of DNDC (Zhang et al., 2018). The CNMM-DNDC



85 has been gradually developing into a comprehensive and reliable process-oriented biogeochemical  
86 model that performs well in terms of simulating the complex hydrologic and biogeochemical processes  
87 of a subtropical catchment with various landscapes (Zhang et al., 2018), the nitrous oxide and nitric  
88 oxide emissions from a subtropical tea plantation (Zhang et al., 2020) and the  $\text{NO}_3^-$  leaching processes  
89 of black soils in northeastern China (Zhang et al., 2021). However, the rationality of the  
90 CNMM-DNDC's scientific processes in simulating  $\text{NH}_3$  volatilization from fertilized croplands is still  
91 lacking in terms of a thorough assessment. In particular, CNMM-DNDC and other widely used  
92 biogeochemical models (e.g., DNDC) do not consider floodwater over rice paddy soils when  
93 simulating  $\text{NH}_3$  volatilization but rather directly adopt the scientific processes and algorithms applied  
94 in  $\text{NH}_3$  volatilization from cultivated uplands to predict  $\text{NH}_3$  volatilization from rice paddy fields (Li,  
95 2016; Zhang et al., 2018).

96 Based on the above deficiencies, the authors hypothesized that the CNMM-DNDC is able to  
97 simulate  $\text{NH}_3$  volatilization following the application of synthetic nitrogen fertilizers to cultivated  
98 uplands and flooded rice paddy fields. To test this hypothesis, this study evaluated and modified the  
99 CNMM-DNDC's scientific processes for simulating  $\text{NH}_3$  volatilization from cropland soils using 44  
100 and 19 fertilizer application events from cultivated uplands and rice paddy fields in China, respectively.  
101 The objectives of this study were to (i) evaluate the performance of the CNMM-DNDC in simulating the  
102 observed  $\text{NH}_3$  volatilization following synthetic nitrogen application to cultivated uplands, (ii) introduce  
103 thoroughly tested and validated scientific algorithms simulating  $\text{NH}_3$  volatilization from cultivated  
104 uplands into the CNMM-DNDC, (iii) adopt widely applied process-based algorithms (J-M model) into  
105 the modified CNMM-DNDC, (iv) assess the performance of the modified model to simulate  $\text{NH}_3$   
106 volatilization from flooded rice paddy fields using collected reliable observations, and (v) identify the  
107 major factors affecting  $\text{NH}_3$  volatilization from uplands and rice paddy fields to offer suggestions for  
108 further improving the model performance.

## 109 **2. Materials and methods**

### 110 **2.1 Brief description of the field sites and treatments**

111 Two field observation datasets of  $\text{NH}_3$  volatilization using micrometeorological methods or wind



112 tunnel techniques, which were measured in cultivated uplands and flooded rice paddy fields of China,  
113 respectively, were collected from published peer-reviewed articles. For the dataset of cultivated uplands,  
114 the collected field observations were conducted at seven experimental sites, including Dongbeiwang  
115 (DBW) in Beijing; Fengqiu with uplands (FQU) in Henan; Guangchuan (GC) Luancheng (LC), and  
116 Quzhou (QZ) in Hebei; Yanting (YT) in Sichuan; and Yongji (YJ) in Shanxi (Fig. 1), and the dataset  
117 were directly inherited from Li et al. (2019). The upland sites involved in this study were calcareous  
118 soils cultivated with summer maize and winter wheat. The 44 cases of synthetic fertilizer application  
119 events in the cultivated uplands involved various fertilizer types (including urea, ammonium  
120 bicarbonate (ABC), ammonium sulfate, and complex fertilizer), a wide range of applied fertilizer doses  
121 ( $60\text{--}348\text{ kg N ha}^{-1}$ ), and various agricultural management practices (e.g., broadcast or deep point  
122 placement of fertilizer(s) alone or fertilization coupled with irrigation). For the rice paddy field dataset,  
123 field observations were collected at five experimental sites, including Changshu (CS) and Danyang  
124 (DY) in Jiangsu, Fengqiu with rice paddy fields (FQP) in Henan, Shenzhen (SZ) in Guangdong, and  
125 Yingtan (YTA) in Jiangxi (Fig. 1), and these sites were cultivated with summer rice and winter wheat  
126 or double rice (Table 1). In total, nineteen (P1–P19) synthetic fertilizer application events were  
127 included in these measurements, covering different fertilizer types, including urea and ABC; fertilizer  
128 doses in the range of  $41\text{--}162\text{ kg N ha}^{-1}$ ; and various agricultural management practices (e.g.,  
129 broadcasting or broadcasting followed by tillage, Table 1 and Table 2). In addition, the other auxiliary  
130 variables, e.g., temperature, pH, and ammonium ( $\text{NH}_4^+$ ) concentration of the floodwater, measured in  
131 the rice paddy experimental sites during the  $\text{NH}_3$  volatilization measurement periods were also  
132 collected for model calibration and validation.

## 133 **2.2 Model introduction and modifications**

### 134 **2.2.1 Brief introduction of the CNMM-DNDC**

135 The CNMM-DNDC used in this study was first established by Zhang et al. (2018) by  
136 incorporating the core biogeochemical processes (including decomposition, nitrification, denitrification  
137 and fermentation) of DNDC (Li, 2016; Li et al., 1992) into the distributed hydrologic framework of  
138 CNMM (Li et al., 2017). Based on comprehensive observations, the CNMM-DNDC was initially tested



139 in a subtropical catchment, which showed credible performances in simulating the yields of crops,  
140 emissions of greenhouse gases (i.e., methane and nitrous oxide), emissions of nitrogenous pollutant  
141 gases (i.e., nitric oxide and ammonia), and hydrological nitrogen losses by leaching and  $\text{NO}_3^-$  discharge  
142 in streams for different land uses (including forests and arable lands cultivated with maize, wheat, oil  
143 rape, or rice paddy) (Zhang et al., 2018). Subsequently, Zhang et al. (2020) modified the  
144 CNMM-DNDC by adding tea growth-related processes that may induce a soil pH reduction, and this  
145 modified model performed well in simulating the emissions of nitrous oxide and nitric oxide from a  
146 subtropical tea plantation plot. Moreover, the CNMM-DNDC performed well in simulating the  $\text{NO}_3^-$   
147 leaching process of black soils in northeastern China (Zhang et al., 2021). However, during model  
148 preparation and operation for the simulation of  $\text{NH}_3$  volatilization, the authors found that the present  
149 model version, using a complicated and obscure R programming script to prepare the ARC GRID  
150 ASCII data format of site/plot-scale inputs, was time-consuming and confusing. Therefore, an  
151 easy-to-operate and standardized version of the model needed to be established. Thus, a standardized  
152 model version was established in this study.

153 The new version of the model was built without changing the original key scientific modules;  
154 however, the complicated R programming script was converted into a simple Excel spreadsheet to  
155 prepare the model inputs, which is easy for beginners to use. The site-scale and regional-scale  
156 simulations were separated. In the site-scale simulation used in this study, the authors hypothesized a  
157 flat terrain region with a  $5 \times 5$  grid, and thus, the solar radiation was not affected by topography.  
158 Therefore, the simulation of any grid was the same and could be regarded as the representative  
159 simulation results of the study region. If the users were only interested in the simulation of a field site  
160 experiment or could only provide the input data based on the site/plot scale, then they would not need  
161 to provide any information about the topography and stream of their study region. This site-scale  
162 simulation is convenient for model validation, saves time in terms of model operation, and is easy to  
163 use for beginners.

#### 164 **2.2.2 Modifications for simulating ammonia volatilization from uplands**

165 The modifications of the new version of the CNMM-DNDC for simulating  $\text{NH}_3$  volatilization



166 from uplands were mainly adapted from Li et al. (2019). Compared to the original CNMM-DNDC, the  
167 authors conducted three major modifications in terms of the new version. First, the parameters of the  
168 urea hydrolysis function were recalibrated. Second, the regulatory effect of soil temperature on ABC  
169 decomposition was parameterized. Finally, the effects of the original parameters of wind, soil  
170 temperature and moisture on  $\text{NH}_3$  volatilization were recalibrated, and the effects of the clay fraction,  
171 plant standing, and canopy wetting on  $\text{NH}_3$  release to the atmosphere were newly parameterized (Fig.  
172 S1). Therefore, the ammonia flux from uplands ( $\text{flux}(\text{NH}_3)_{\text{uplands}}$ ) was jointly determined by the  
173 regulating factors of wind speed ( $f_{\text{wind}}$ , 0–1), soil temperature ( $f_{\text{temp}}$ , 0–1), soil moisture ( $f_{\text{water}}$ , 0–1), soil  
174 depth ( $f_{\text{depth}}$ , 0–1), clay fraction ( $f_{\text{clay}}$ , 0–1), vegetation canopy ( $f_{\text{canopy}}$ , 0–1), and rainfall-induced canopy  
175 wetting ( $f_{\text{rain}}$ , 0–1), as shown in Eq. (1).  $\text{NH}_{3(l)}$  is referred to as the dissolved  $\text{NH}_3$  in the liquid phase of  
176 upland soils. Among these regulating factors,  $f_{\text{depth}}$  was calculated by the number of soil layers in Li et  
177 al. (2019), where the thickness of the soil layer was set as the value of the saturated hydraulic  
178 conductivity. However, in the CNMM-DNDC, the simulated soil layers and their corresponding  
179 thicknesses were set to be freely defined by users. The algorithm of  $f_{\text{depth}}$  from Li et al. (2019) was  
180 inappropriate for this study. Therefore,  $f_{\text{depth}}$  was revised using the thickness of the soil layer based on  
181 Eq. (2), wherein  $d_s$  denotes the depth of the simulated soil layer. Moreover, the time step of the  
182 CNMM-DNDC was three hours, but the time step was one day in the DNDC model. To solve the  
183 simulation deviation derived from the different time steps, a time-step parameter ( $f_{\text{Tstep}}$ , 0–1) was  
184 introduced into Eq. (1), which was calculated at 0.75 in this study.

$$\text{Flux}(\text{NH}_3)_{\text{upland}} = 3.6f_{\text{wind}}f_{\text{temp}}f_{\text{water}}f_{\text{depth}}f_{\text{clay}}f_{\text{canopy}}f_{\text{rain}}f_{\text{Tstep}}\text{NH}_{3(l)} \quad (1)$$

$$f_{\text{depth}} = 0.5^{d_s/0.03} \quad (2)$$

185

### 186 2.2.3 Modifications for simulating ammonia volatilization from rice paddy fields

187 The original CNMM-DNDC failed to simulate  $\text{NH}_3$  volatilizations from rice paddy fields because  
188 it lacked the capability to simulate the surface water-flooded layer over rice paddy fields. Given the  
189 presence of floodwater over rice paddy soils, the mechanisms of  $\text{NH}_3$  volatilization are different  
190 between uplands and rice paddy fields. However, CNMM-DNDC and other widely used



191 biogeochemical models (e.g., DNDC) adopted scientific processes and algorithms applied in simulating  
192  $\text{NH}_3$  volatilization from fertilized cultivated uplands to calculate  $\text{NH}_3$  volatilization from rice paddy  
193 fields without considering floodwater over soils (Cannavo et al., 2008; Li, 2016). Therefore, floodwater  
194 over rice paddy soils was added to the modified CNMM-DNDC. To add this component, the modified  
195 CNMM-DNDC adopted the Jayaweera-Mikkelsen model (i.e., J-M model), based on the two-film  
196 theory of mass transfer (Jayaweera and Mikkelsen, 1990a), which is one of the most widely applied  
197 process-based models for simulating  $\text{NH}_3$  volatilization from rice paddy fields. The J-M model consists  
198 of two processes (Fig. 2): (i) the chemical processes of  $\text{NH}_4^+$  ions and aqueous  $\text{NH}_3$  ( $\text{NH}_{3(\text{aq})}$ )  
199 equilibrium in floodwater and (ii) the volatilization processes of  $\text{NH}_{3(\text{aq})}$  transfer in the form of  $\text{NH}_3$  gas  
200 ( $\text{NH}_{3(\text{air})}$ ) across the water-air interface to the atmosphere (Rxn1).  $k_d$  (first-order,  $\text{s}^{-1}$ ) and  $k_a$   
201 (second-order,  $\text{L mol}^{-1} \text{s}^{-1}$ ) are referred to as the dissociation and association rate constants for  
202  $\text{NH}_4^+/\text{NH}_{3(\text{aq})}$  equilibrium, respectively.  $k_{vN}$  (first-order,  $\text{s}^{-1}$ ) is referred to as the volatilization rate  
203 constant of  $\text{NH}_{3(\text{aq})}$ .



204 According to the above theories, the change rate of the  $\text{NH}_4^+$  concentration in floodwater ( $[\text{NH}_4^+]_w$ ,  
205  $\text{mol L}^{-1}$ ) due to  $\text{NH}_3$  volatilization ( $R_a$ ,  $\text{mol L}^{-1} \text{s}^{-1}$ ) can be estimated by Eq. (3) as a function of  
206  $[\text{NH}_4^+]_w$ ,  $\text{H}^+$  concentration in floodwater ( $[\text{H}^+]_w$ ,  $\text{mol L}^{-1}$ ),  $k_d$ ,  $k_a$  and  $k_{vN}$ .

$$R_a = -\frac{k_d k_{vN} [\text{NH}_4^+]_w}{k_a [\text{H}^+]_w + k_{vN}} \quad (3)$$

207 The dynamic changes in  $[\text{H}^+]_w$  and  $[\text{NH}_4^+]_w$  are calculated by the CNMM-DNDC instead of the  
208 field experiment described in Jayaweera and Mikkelsen (1990a).

209 In the modified CNMM-DNDC, the pH of the floodwater, which is the negative logarithm of  
210  $[\text{H}^+]_w$ , is related to the initial pH of water for flooding and that of surface soil. When the floodwater  
211 depth is less than 0.04 m, the pH of the floodwater is equal to the mean of the initial pH of water for  
212 flooding and that of surface soil, both of which are the inputs of the modified model. Otherwise, the pH  
213 of the floodwater is equal to the initial pH of the water for flooding. On the one hand,  $[\text{H}^+]_w$  is regulated  
214 by urea hydrolysis in floodwater, the algorithm of which was derived from that of urea hydrolysis  
215 affecting soil pH in the model. On the other hand, many studies have found that a marked diurnal



216 fluctuation in floodwater pH is associated with algal photosynthesis, which was elevated with solar  
217 radiation (De Datta, 1995; Fillery and Vlek, 1986). Therefore, a ratio of the daytime solar shortwave  
218 radiation effect on algal photosynthesis ( $R_{\text{slr}}, 0-1$ ) was established by the authors using Eq. (4) as a  
219 quadratic function of the simulation time ( $t$ , 06:00 to 21:00 with a 3-hour interval) of a day.  $R_{\text{slr}}$  at the  
220 other moments with no or extremely little solar radiation in a day was set as 0. The effect of algal  
221 growth ( $f_{\text{alg}}$ ) on floodwater pH was calculated by Eq. (5), where the adjusted coefficient ( $k_{\text{alg}}, 0-1$ ) was  
222 calibrated to 0.75 or 0.6 when the floodwater depth was no more than or more than 0.04 m, respectively.  
223 The floodwater pH of  $(t+1)$ th was modified by the floodwater pH of  $t$ th and  $f_{\text{alg}}$  using Eq. 6, which was  
224 set as no more than 10.

$$R_{\text{slr}} = -0.0036t^2 + 0.1096t - 0.7046 \quad (4)$$

$$f_{\text{alg}} = k_{\text{alg}}R_{\text{slr}}R + 0.25 \quad (5)$$

$$\text{pH}_{t+1} = \text{pH}_t + f_{\text{alg}} \quad (6)$$

225 When fertilizers (e.g., urea) are applied to the rice paddy fields, they are first allocated to the  
226 floodwater and soil layers according to the ratio of the floodwater depth and the application depth of  
227 fertilizer in the modified CNMM-DNDC. Subsequently,  $[\text{NH}_4^+]_w$  increases with urea hydrolysis, and  
228 ABC decomposition occurs in the floodwater. In the modified model, the calculation of urea hydrolysis  
229 in floodwater refers to that in the upland soils (Dubache et al., 2019) by removing the influencing  
230 factors of soil organic carbon and soil moisture. Therefore, urea hydrolysis in floodwater is only  
231 determined by the floodwater temperature. To simplify the calculation, the floodwater temperature is  
232 arbitrarily set equal to the temperature in the first soil layer in the modified model. Given that ABC  
233 decomposition in floodwater was not involved in the original CNMM-DNDC, this study directly  
234 adopted the algorithm of ABC decomposition in upland soils used in Li et al. (2019), and this process  
235 was regulated by soil temperature, pH and the applied depth of fertilizer. However, ABC decomposition  
236 in floodwater is different from that in upland soils; i.e., the ABC concentration is uniformly distributed  
237 in the floodwater, and the effect factors (i.e., temperature, pH and depth) applied should be those of  
238 floodwater rather than those of soil. Therefore, this study ignored the effect of soil depth and retained



239 the effect of floodwater temperature and pH on ABC decomposition in floodwater.

240 For each simulation time step, the  $\text{NH}_4^+$  in the floodwater and the first soil layer experiences  
241 uniform mixing and exchange. Then,  $\text{NH}_4^+$  is transported in soil layers, accompanied by organic  
242 nitrogen mineralization, consumption via plant uptake, nitrification, volatilization of  $\text{NH}_3$ , and  
243 adsorption/desorption by clay (Li, 2016; Li et al., 1992; Li et al., 2019).

244  $k_d$ ,  $k_a$  and  $k_{vN}$  in Eq. (3) are determined by the environmental factors, i.e., the temperature and the  
245 depth of floodwater (Jayaweera and Mikkelsen, 1990a). As shown in Eq. (7),  $k_a$  is affected by its  
246 relationship with floodwater temperature ( $T_f$ , K) based on Albery (1983):

$$k_a = 3.8 \times 10^{11} - 3.4 \times 10^9 T_f + 7.5 \times 10^6 T_f^2 \quad (7)$$

247  $k_d$  is derived from the relationship with the equilibrium constant for  $\text{NH}_4^+/\text{NH}_3(\text{aq})$  ( $K$ ) and  $k_a$  (Eq.  
248 (8)):

$$k_d = K k_a \quad (8)$$

249  $K$  is calculated as a function of the floodwater temperature (Eq. (9)) derived from Jayaweera and  
250 Mikkelsen (1990a):

$$K = 10^{-[0.0897 + (2729/T_f)]} \quad (9)$$

251 The  $\text{NH}_3$  volatilization rate constant ( $k_{vN}$ ) is estimated by the law of conservation of mass, which  
252 is considered in the system of  $\text{NH}_3$  transfer across the air-water interface. By dimensional analysis,  $k_{vN}$   
253 is determined by Eq. (10), based on the ratio of the floodwater depth ( $d$ , m) and the overall  
254 mass-transfer coefficient for  $\text{NH}_3$  ( $K_{ON}$ ,  $\text{cm h}^{-1}$ ):

$$k_{vN} = K_{ON} / (3.6 \times 10^5 d) \quad (10)$$

255 According to the two-film theory, based on Fick's first law and Henry's law,  $K_{ON}$  is determined by  
256 Eq. (11) using the exchange constant for  $\text{NH}_3$  in the gas and liquid phases ( $k_{gN}$  and  $k_{lN}$ , respectively)  
257 and the non-dimensional Henry's constant ( $H_{nN}$ ). As described by Jayaweera and Mikkelsen (1990a),  
258  $H_{nN}$  is a function of  $T_f$ , which can be calculated by Eq. (12), whereas  $k_{gN}$  and  $k_{lN}$  are dependent on the  
259 wind speed measured at a height of 8 m ( $U_8$ ,  $\text{m s}^{-1}$ ), which can be calculated using Eqs. (13–14).  $U_8$



260 can be determined using the model input of wind speed measured at a height of 10 m ( $U_{10}$ ,  $\text{m s}^{-1}$ ),  
261 based on Eq. (15) derived from Jayaweera and Mikkelsen (1990a).

$$K_{\text{ON}} = (H_{\text{nN}}k_{\text{gN}}k_{\text{IN}})/(H_{\text{nN}}k_{\text{gN}} + k_{\text{IN}}) \quad (11)$$

$$H_{\text{nN}} = 183.8e^{(-1229/T_f)}/RT_f \quad (12)$$

$$k_{\text{gN}} = 19.0895 + 742.3016U_8 \quad (13)$$

$$k_{\text{IN}} = \left\{ 12.5853 / \left[ 1 + 43.0565e^{(-0.4417U_8)} \right] \right\} / 1.6075 \quad (14)$$

$$U_8 = \frac{11.51}{\ln(10/8 \times 10^5)} U_{10} \quad (15)$$

262 Finally, the three-hour cumulative flux of  $\text{NH}_3$  volatilization ( $\text{Flux}(\text{NH}_3)_{\text{rice}}$ ,  $\text{kg N ha}^{-1} 3\text{h}^{-1}$ ) is  
263 calculated by Eq. (16) using  $R_a$ ,  $d$ , and the simulation time step based on the molar mass of N ( $\sim 14$  g  
264  $\text{mol}^{-1}$ ) and the conversion coefficient from  $\text{m}^2$  to ha ( $1 \text{ m}^2 = 1 \times 10^{-4} \text{ ha}$ ).

$$\text{Flux}(\text{NH}_3)_{\text{rice}} = -1.512 \times 10^9 dR_a \quad (16)$$

265 The CNMM-DNDC with the above modifications is hereinafter referred to as the modified  
266 CNMM-DNDC. The cases for model calibration were identified on the basis of covering as many  
267 climate conditions, soil properties and management practices as possible. Therefore, for the simulation  
268 of  $\text{NH}_3$  from urea application on uplands and rice paddy fields, 26 typical cases of DBW, FQU, and QZ  
269 and 10 typical cases of DY, FQP, and SZ were used for model calibration. Regarding the simulation of  
270  $\text{NH}_3$  from the ABC application on uplands and rice paddy fields, 3 typical cases of DBW and YT and 1  
271 typical DY case were conducted for model calibration. The remaining 23 independent cases were  
272 provided for model validation.

## 273 2.3 Model preparation and operation

### 274 2.3.1 Input data formatting

275 The input data of the modified CNMM-DNDC used in this study included the meteorological  
276 conditions of the study area (e.g., 3-hourly average air temperature ( $T_{\text{air}}$ ), precipitation ( $P$ ), wind speed  
277 ( $W$ ), solar radiation ( $R$ ), relative humidity (RH)), the necessary soil properties of individual layers (e.g.,



278 soil clay and sand fraction, organic carbon (SOC), bulk density (BD), pH), crop parameters (e.g., crop  
279 type, thermal degree days for maturity (TDD), nitrogen content, plant height and root depth), and the  
280 implemented management practices (e.g., plant and harvest dates, methods and/or amounts of  
281 individual management practices including fertilization, tillage, irrigation and flooding).

282 For the meteorological data inputs, the reported 3-hourly meteorological data from the weather  
283 station at the experimental site were used. If these data were not available, then data from the adjacent  
284 weather station in the China Meteorological Administration (CMA, <http://www.data.cma.cn>) were  
285 adapted by referring to the reported average or maximum values (Table S1, Text S1).

286 The necessary inputs of surface soil properties at the individual upland sites for the modified  
287 model were derived from Li et al. (2019), whereas those at the individual rice paddy sites are shown in  
288 Table S2. If the observed surface soil properties were not available, then the values were provided  
289 using the methods of Li et al. (2019). The soil clay and sand fraction and pH in the deep layers were set  
290 to be consistent with those in the surface soil. Depending on the SOC at the surface soil, the modified  
291 CNMM-DNDC calculated the SOC in the deep layers using the algorithms involved in Li (2016), and  
292 the BD in the deep layers were estimated using the SOC value in the corresponding layers based on the  
293 algorithms shown in Li (2016). Other soil properties (e.g., field capacity, wilting point and saturated  
294 hydraulic conductivity) were estimated using the pedo-transfer functions of Li et al. (2019).

295 The CNMM-DNDC contains a library of crop parameters. However, to ensure the normal growth of  
296 the crop(s), the model's default values for the crop TDD at the individual sites were adapted by the  
297 multiyear (at least five years) average of the sums of daily air temperatures during the growing season.

298 Agricultural management practice information included in the CNMM-DNDC input was  
299 organized on a daily scale. The management practice information for the cases of uplands was derived  
300 from Li et al. (2019), whereas that for the cases of rice paddy fields is listed in Table S3. It is worth  
301 noting that the information input for the cases of rice paddy fields required the start and end dates of  
302 the individual flooding events accompanied by the corresponding pH and depth of floodwater as model  
303 inputs. The default value of the initial floodwater pH at all sites was set at 7.0 due to a lack of  
304 observations. The cases in DY, FQP and YT had reported floodwater depth observations, and the cases  
305 of CS without floodwater depth observations were arbitrarily set to the traditional floodwater depth



306 (0.04 m) of the DY site, which was located in the same region. For the SZ cases without floodwater  
307 depth observations, given that no site is adjacent to the Pearl River Delta region where SZ is located,  
308 the floodwater depth of the SZ site was calculated at 0.075 m.

### 309 **2.3.2 Model operation**

310 To reduce the influences of initial model inputs, the model simulation consists of a spin-up period  
311 conducted for at least five years (depending on the availability of the model inputs) and the  
312 corresponding experimental period. The sources of the daily meteorological data for the spin-up period  
313 and the following simulation for upland and rice paddy field sites were derived from Li et al. (2019) and  
314 listed in Table S4, respectively.

### 315 **2.4 Sensitivity analysis**

316 Sensitivity analysis was adopted to investigate the regulating factors in the modified  
317 CNMM-DNDC that simulates  $\text{NH}_3$  volatilization following fertilizer application. Meteorological  
318 variables (i.e., 3-hourly averages of  $T_{\text{air}}$  and  $W$ ; 3-hourly totals of  $P$  and  $R$  during measurement periods  
319 of  $\text{NH}_3$  volatilization), soil properties (i.e., soil clay fraction, pH, SOC content and BD), and field  
320 management practices (i.e., water management (irrigation water amount or depth of floodwater) and  
321 nitrogen fertilization type, dose and depth) were involved in this sensitivity test. U37 in QZ and P4 in  
322 CS were chosen as the baseline cases to assess the model's behavior in simulating  $\text{NH}_3$  volatilization  
323 from uplands and rice paddy fields, respectively. One reason for this selection was that U37 and P4  
324 were geographically located near the center of the region for upland and rice paddy cases, respectively.  
325 Another reason was that the selected cases implement general Chinese management practices. The  
326 authors altered only one item at a time by maintaining the others constant. The model input items of the  
327 3-hourly average of  $W$ , 3-hourly totals of  $P$  and  $R$  during the measurement periods of  $\text{NH}_3$   
328 volatilization, as well as the soil clay fraction, SOC content, nitrogen fertilization dose, and depth of  
329 floodwater, were increased by a range from  $-30\%$  to  $+30\%$  with an interval of  $10\%$ . Soil BD and pH,  
330 with narrow amplitudes in situ, were altered within the ranges of 1.17 to 1.47 (U37) and 0.89 to 1.19  
331 (P4) with an interval of 0.05 and within the ranges of 7.3 to 8.9 (U37) and 6.2 to 8.1 (P4) with an  
332 interval of 0.3, respectively. The 3-hourly average  $T_{\text{air}}$  during the measurement period of  $\text{NH}_3$



333 volatilization was altered within the range of  $-3\text{ }^{\circ}\text{C}$  to  $+3\text{ }^{\circ}\text{C}$  with an interval of  $1\text{ }^{\circ}\text{C}$ . The irrigation  
334 water amount and nitrogen fertilization depth and type were set as 0.2/0.5/5 cm, 5/10/15 cm and  
335 ABC/ammonium-based nitrogen (N) fertilizers excluding ABC, respectively. The corresponding  
336 baselines and lower/upper bounds of the above items involved in the sensitivity analysis are listed in  
337 Table S5. The change ratios of cumulative  $\text{NH}_3$  volatilization during the measurement periods between  
338 the lower/upper and baseline simulations were applied as the quantitative evaluation index for the  
339 sensitivity analysis (Abdalla et al., 2020).

#### 340 **2.5 Evaluation of model performance and statistical analysis**

341 The index of agreement (IA), Nash–Sutcliffe Index (NSI), relative model bias (RMB), as well as  
342 slope, significance level and coefficient of determination ( $R^2$ ) of the zero-intercept linear regression  
343 (ZIR) between the observed ( $O$ ) and simulated ( $S$ ) values were applied to quantitatively assess the  
344 performance of the original and modified models. The algorithms of these statistical metrics refer to Li  
345 et al. (2019). If the slope and  $R^2$  of the zero-intercept linear regression as well as the IA and NSI values  
346 are closer to 1, then the model performance is better. The SPSS Statistics Client 19.0 (SPSS Inc.,  
347 Chicago, USA) software package was used for the multiple regression analysis. The Origin 8.0  
348 (OriginLab Ltd., Guangzhou, China) software package was used for graph drawing.

### 349 **3. Results**

#### 350 **3.1 Ammonia volatilization from uplands**

351 The observed cumulative ammonia volatilization (CAV) in all the cases of the uplands during the  
352 measurement periods totaled  $0.6\text{--}127.7\text{ kg N ha}^{-1}$  (mean:  $27.5\text{ kg N ha}^{-1}$ ). The corresponding CAVs  
353 simulated by the original and modified CNMM-DNDC totaled  $0.5\text{--}94.1\text{ kg N ha}^{-1}$  (mean:  $33.2\text{ kg N}$   
354  $\text{ha}^{-1}$ ) and  $0.8\text{--}115.2\text{ kg N ha}^{-1}$  (mean:  $27.8\text{ kg N ha}^{-1}$ ), respectively (Table S6). The original  
355 CNMM-DNDC performed poorly in simulating all the observed cumulative  $\text{NH}_3$  volatilization cases,  
356 showing an acceptable IA (0.55), an unacceptable NSI ( $-1.49$ ) and an insignificant ZIR (slope = 1.11  
357 and  $R^2 = 0.06$ ) (data not shown).

358 In this study, several modifications were conducted to improve the CNMM-DNDC performance in



359 simulating  $\text{NH}_3$  volatilizations from upland soils. Regarding either the typically calibrated or  
360 independently validated cases, the modified CNMM-DNDC did not perform well in simulating daily  
361  $\text{NH}_3$  fluxes, with low IA and unacceptable NSI values (Table 3). This result was probably because the  
362 simulated  $\text{NH}_3$  dynamic peak time could not absolutely be matched to the observed peak time, although  
363 the modified model captured the observed  $\text{NH}_3$  dynamic trend. For the 3 only typically calibrated ABC  
364 cases, the modified model performed marginally well in simulating CAVs, showing a good IA (0.75)  
365 but a low NSI (0.14) and an insignificant ZIR ( $R^2 = 0.64$ ) (Table 3). However, the modified model  
366 showed a perfect performance in simulating CAVs of both the calibrated and validated urea cases, with  
367 IA values (0.93 and 0.91) close to 1, acceptable NSI values (0.73 and 0.49), and significant ZIRs ( $R^2 =$   
368  $0.71$  with slope = 0.94 and  $R^2 = 0.74$  with slope = 1.06) (Table 3). Regarding the CAVs of all the  
369 individual cases of uplands, the modified model reported an |RMB| of 1.0–307.8% (mean: 69.8%, Table  
370 2), with only 16% (seven of forty-four) of cases suffering from an |RMB| larger than 100%.

### 371 **3.2 Ammonia volatilization from rice paddy fields**

372 The observed CAVs in all cases of rice paddy fields (2 and 17 cases for ABC and urea applications,  
373 respectively) during the measurement periods totaled 5.9–39.8  $\text{kg N ha}^{-1}$  (mean: 18.1  $\text{kg N ha}^{-1}$ , Table  
374 2), with fertilizer application doses of 40.5–162.2  $\text{kg N ha}^{-1}$  (mean: 81.4  $\text{kg N ha}^{-1}$ ). Given the lack of  
375 the capacity to simulate the water-flooded layer over rice paddy fields, the original CNMM-DNDC  
376 could not simulate  $\text{NH}_3$  volatilizations from rice paddy fields. The corresponding CAVs simulated by  
377 the modified CNMM-DNDC totaled 3.4–39.1  $\text{kg N ha}^{-1}$  (mean: 16.2  $\text{kg N ha}^{-1}$ , Table 2). Regarding the  
378 CAVs of all the individual cases of rice paddy fields, the modified model demonstrated an |RMB| of  
379 0.3–94.9% (mean: 32.7%, Table 2), and none of nineteen cases showed an |RMB| larger than 100%.  
380 With regard to the only two ABC cases, the simulated daily  $\text{NH}_3$  fluxes generally matched the  
381 observations of the typically calibrated and independently validated cases (P1 and P2, respectively),  
382 although the simulated peak emissions of the first day for P1 were lower than the observations (Fig.  
383 3e–f). For P1 and P2, the corresponding statistical indices showed that IA values were 0.33 and 0.94,  
384 the NSI values were 0.02 and 0.85, and the ZIR slopes were 0.16 (not available  $R^2$  and  $p$  values,  $n = 7$ )  
385 and 0.90 ( $R^2 = 0.71$ , not significant,  $n = 4$ ), respectively (Table 3). The observed and simulated daily



386 NH<sub>3</sub> fluxes due to urea application in the individual cases are illustrated in Fig. 4c–f and Fig.5i–k,  
387 respectively. As the figures demonstrate, the temporal NH<sub>3</sub> flux variation pattern simulated by the  
388 modified model generally followed that observed in the field. Regarding the simulations of the 10  
389 typically calibrated and 7 independently validated urea cases, the modified model did not show good  
390 performance in terms of the daily NH<sub>3</sub> flux, with IA values of 0.53 and 0.72, NSI values of –0.35 and 0.  
391 36 and ZIR slopes of 0.47 ( $R^2 = 0.04$ ,  $p < 0.05$ ,  $n = 176$ ) and 0.56 ( $R^2 = 0.19$ ,  $p < 0.001$ ,  $n = 63$ ),  
392 respectively (Table 3). However, the modified CNMM-DNDC performed extremely well in simulating  
393 CAVs of the calibrated and validated urea cases, showing good IA values of 0.88 and 0.85, acceptable  
394 NSI values of 0.30 and 0.60, and significant ZIR slopes of 1.03 ( $R^2 = 0.68$ ,  $n = 10$ ) and 0.77 ( $R^2 = 0.65$ ,  
395  $n = 7$ ), respectively (Table 3).

396 As Fig. 6 shows, with regard to the simulations of all 40 typically calibrated and 23 independently  
397 validated cases of uplands and rice paddy fields by the modified model, significant zero-intercept linear  
398 relationships between the simulated and observed CAVs were found, with slopes of 0.94 ( $R^2 = 0.76$ )  
399 and 0.98 ( $R^2 = 0.71$ ), respectively. In general, the above results indicated that the modifications made in  
400 this study obviously improved the performance of the CNMM-DNDC in simulating NH<sub>3</sub> volatilization  
401 following applications of synthetic nitrogen fertilizers to upland and rice paddy soils.

### 402 3.3 Model performance in terms of other auxiliary variables in rice paddy fields

403 Table 4 lists the statistical indices used to evaluate the performance of the modified  
404 CNMM-DNDC in the simulation of floodwater temperatures, pH values and NH<sub>4</sub><sup>+</sup> concentrations when  
405 the model was calibrated and validated. The modified model generally captured the trends in  
406 floodwater temperature (Fig. 5a–b), although the simulated floodwater temperatures of several certain  
407 days for P9 were lower than the observations. The modified CNMM-DNDC, which introduced the  
408 effect of algal growth on floodwater pH, generally simulated the observed daily elevated floodwater pH  
409 resulting from algal photosynthetic activity (Fig. 3a–b and Fig. 5c–e). The simulation of calibrated (P1,  
410 P9 and P10, Fig. 3a and Fig. 5c–d) and validated cases (P2 and P19, Fig. 3b and Fig. 5e) of floodwater  
411 pH resulted in good IA values of 0.83 and 0.79, acceptable NSI values of 0.55 and 0.36, and ZIRs with  
412 significant  $R^2$  values of 0.55 (slope = 1.00,  $n = 147$ ) and 0.36 (slope = 1.01,  $n = 45$ ), respectively. The



413 simulated and observed daily  $\text{NH}_4^+$  concentrations in the floodwater of the ABC and urea cases are  
414 illustrated in Fig. 3c–d, Fig. 4a–b and Fig. 5f–h. Compared to the observed floodwater  $\text{NH}_4^+$   
415 concentrations of the ABC cases, the model simulation underestimated the peak concentration on the  
416 first day after ABC application for the P1 case but captured the peak concentration of the P2 case (Fig.  
417 3c–d). The modified CNMM-DNDC generally captured the observed temporal pattern in the daily  
418  $\text{NH}_4^+$  concentrations during the observation periods following urea application, although discrepancies  
419 existed in the magnitudes of some cases; e.g., the model overestimated the floodwater  $\text{NH}_4^+$   
420 concentration in the P7 and P8 cases (Fig. 4a–b) and underestimated that in the P6 (Fig. 4b) and P19  
421 cases (Fig. 5h). Significant ZIRs between the simulated and observed daily floodwater  $\text{NH}_4^+$   
422 concentrations of the typically calibrated and independently validated cases yielded significant slopes  
423 of 1.03 ( $R^2 = 0.48$ ,  $n = 24$ ) and 0.74 ( $R^2 = 0.34$ ,  $n = 55$ ), the IA values were 0.78 and 0.68, and the NSI  
424 values were 0.48 and 0.25, respectively (Table 4).

#### 425 **3.4 Regulating factors of the modified model in simulating ammonia volatilization**

426 The sensitivity analysis indicated that  $\text{NH}_3$  volatilization from upland soils was primarily  
427 regulated by field management practices (Fig. 7a). The changes in N dose, the different N types and the  
428 implementation of irrigation had considerable effects on  $\text{NH}_3$  volatilization from upland soils. In  
429 addition, a fertilization depth of 15 cm resulted in a –23% change in  $\text{NH}_3$  volatilization, and the  
430 increase in irrigation amount had an inhibitory effect on  $\text{NH}_3$  volatilization. Moreover, in comparison to  
431 other soil properties, the changes in soil SOC had a greater influence (–19% to 16%) on  $\text{NH}_3$   
432 volatilization. Among all considered meteorological variables,  $\text{NH}_3$  volatilization from upland soils  
433 appeared to be the most sensitive response to changes in air temperature (Fig. 7a). However,  $\text{NH}_3$   
434 volatilization from rice paddy soils was sensitive to changes in fertilization and floodwater  
435 management, which increased with N dosage and decreased with the depth of fertilizer application and  
436 that of floodwater (Fig. 7b). For all soil variables considered in the sensitivity analysis, only the  
437 changes in soil pH had a great influence on  $\text{NH}_3$  volatilization from rice paddy soils. In addition,  $\text{NH}_3$   
438 volatilization from rice paddy soils decreased with solar radiation.



439 **4. Discussion**

440 **4.1 Factors affecting ammonia volatilization from uplands**

441  $\text{NH}_3$  volatilization from soil-plant upland systems is an extremely complex process (Freney and  
442 Simpson, 1983; Sommer et al., 2004). The mechanism of  $\text{NH}_3$  volatilization in the modified  
443 CNMM-DNDC is mainly inherited from that in the DNDC model modified by Li et al. (2019). The rate  
444 of ammonia flux is jointly determined by the regulating factors of wind speed, soil depth, clay fraction,  
445 soil temperature, soil moisture, vegetation canopy, and rainfall-induced canopy wetting. It is obvious  
446 that soil properties play an important role in regulating  $\text{NH}_3$  volatilization from upland soils, as has  
447 been reported by a great number of studies (e.g., Duan and Xiao, 2000; Lei et al., 2017; Martens and  
448 Bremner, 1989). In addition, across all the cases of uplands (Table S6), the simulations of the modified  
449 CNMM-DNDC with an RMB larger than 150% occurred in the cases with fertilizer application depth  
450 (U6 with broadcast followed by tillage (BFT) 20 cm, U20 with BFT 5 cm and U44 with deep point  
451 placement 5–10 cm) and irrigation/precipitation (U16 with 4–6 cm irrigation, U22 with 4–6 cm  
452 irrigation and U26 with 0.8 cm irrigation and 3.69 cm precipitation). Compared with all the cases with  
453 fertilizer application depth or irrigation/precipitation (38 cases), the proportion of the cases with RMB  
454 greater than 150% (6 cases) accounted for 16%. This result might be because the model could not  
455 simulate well the inhibition mechanisms of some situations of fertilization depth and water-adding  
456 events effect on  $\text{NH}_3$  volatilization. Moreover, Li et al. (2019) also reported that irrigation/precipitation  
457 during the measurement periods had a complex effect (e.g., reduction and stimulation) on  $\text{NH}_3$   
458 volatilization following nitrogen fertilizer application in cultivated upland soils, and determining this  
459 information is still a considerable challenge in  $\text{NH}_3$  simulations by biogeochemical models. At the  
460 same time, Li et al. (2019) also found that the doses and depths of the fertilizer applications jointly  
461 accounted for 43% ( $p < 0.001$ ) of the variance in the observed CAVs. The results demonstrated that the  
462 simulated  $\text{NH}_3$  volatilization from uplands following nitrogen fertilizer application accompanied with  
463 deep- or mixed-placement or irrigation/precipitation by the modified model still had some deviation  
464 from the observations, and more synchronous observations of  $\text{NH}_3$  volatilization and other auxiliary  
465 variables (e.g., soil moisture,  $\text{NH}_4^+$  concentration and nitrogen uptake by crops) in these situations are  
466 urgently needed to further revise the CNMM-DNDC.



#### 467 4.2 Effects of floodwater on ammonia volatilization from rice paddy fields

468 Floodwater pH has been considered one of the primary factors affecting  $\text{NH}_3$  volatilization from  
469 rice paddy fields (Fillery et al., 1984; Hayashi et al., 2006; Jayaweera and Mikkelsen, 1991). As  
470 floodwater pH increases, the equilibrium of  $\text{NH}_4^+$  ions and  $\text{NH}_{3(\text{aq})}$  in floodwater transfers in the  
471 direction of  $\text{NH}_{3(\text{aq})}$  formation, which will increase the potential for subsequent  $\text{NH}_3$  volatilization  
472 (Jayaweera and Mikkelsen, 1990a; Sommer et al., 2004). In this study, four improvements in the pH of  
473 floodwater were involved in the modified CNMM-DNDC. First, floodwater over rice paddy soil was  
474 added, which enabled the simulation of floodwater pH in the modified model. Second, the modified  
475 model used the initial pH of floodwater and the pH of the surface soil to calculate the floodwater pH.  
476 The above two improvements allowed the introduction of the J-M model into the modified  
477 CNMM-DNDC. The present relatively reliable biogeochemical models rarely involve floodwater over  
478 rice paddy soil when simulating  $\text{NH}_3$  volatilization from rice paddy fields, which is not in accordance  
479 with the natural state. Third, when urea was applied to the surface floodwater, the subsequent urea  
480 hydrolysis reaction could increase the floodwater pH, and this process was added to the modified  
481 model by referring to the algorithms applied in the original model for upland soils (Sec. 2.2.2). Finally,  
482 the effect of algal growth on floodwater pH was introduced into the modified model by calculating the  
483 ratio of the solar shortwave radiation effect on algal photosynthesis. In detail, under cloudy conditions  
484 in DY (P9), only 9% of the applied urea-N was observed to be lost as ammonia from the rice paddy soil,  
485 while up to 40% of the applied urea-N was observed to be lost under high solar radiation conditions in  
486 YTA (P19) (Cai et al., 1992). However, the modified CNMM-DNDC overestimated the emissions from  
487 DY but underestimated those from YTA, which could be attributed to the overestimation of the pH  
488 during the first three observation days in DY and the underestimation of  $\text{NH}_4^+$  concentrations in YTA  
489 (Fig. 5). In addition, algal blooms only appeared on the surface of calm water; thus, a number of factors,  
490 such as irrigation, heavy rain, strong wind, and drainage, could hamper the growth of algae (Cao et al.,  
491 2013). Due to the basal dressing followed by irrigation (Gong et al., 2013), which inhibited the  
492 reproduction of algae in SZ (P11 and P12 cases), the observed ammonia emissions accounted for only  
493 10%–13% of the applied nitrogen. Unfortunately, the aforementioned factors that reduced algal growth  
494 were not introduced into the modified CNMM-DNDC because of limited reports, which resulted in an



495 overestimation of ammonia emissions of 6.4 and 2.6 kg N ha<sup>-1</sup> for P11 and P12 in SZ cases with a high  
496 rate of urea application, respectively. Previous studies have also shown that the stimulation of NH<sub>3</sub>  
497 volatilization from rice paddy fields is affected by algal growth, which largely contributes to the  
498 elevation of floodwater pH resulting from algal photosynthetic activity (Buresh et al., 2008; Fillery and  
499 Vlek, 1986; Mikkelsen et al., 1978). The addition of a suitable photosynthetic inhibitor also controlled  
500 the pH of the floodwater, implying that the increase in pH was caused by algal growth (Bowmer and  
501 Muirhead, 1987). Therefore, more observational data on the effect of algal growth on floodwater pH and  
502 subsequent NH<sub>3</sub> volatilization are needed to improve the simulation of the modified model on NH<sub>3</sub>  
503 volatilization from rice paddy fields.

504 Many studies have found that the depth of surface floodwater has a substantial influence on NH<sub>3</sub>  
505 volatilization (Fillery et al., 1984; Freney et al., 1988; Hayashi et al., 2006). The sensitivity analysis of  
506 this study also indicated that NH<sub>3</sub> volatilization from rice paddy fields was sensitive to changes in the  
507 depth of surface floodwater (Fig. 7b). Jayaweera and Mikkelsen (1990b) demonstrated that the  
508 volatilization rate of NH<sub>3</sub> decreases as the depth of floodwater increases despite the small difference in  
509 meteorological factors and soil physicochemical properties. The reducing effects might be attributed to  
510 the following mechanisms. First, with increasing floodwater depth, the concentration of NH<sub>4</sub><sup>+</sup> in  
511 floodwater decreases (Cai et al., 1986). Many studies have found that a lower concentration of NH<sub>4</sub><sup>+</sup> in  
512 floodwater contributes to the reduced potential of NH<sub>3</sub> volatilization in paddy fields (Bhagat et al.,  
513 1996; Hayashi et al., 2006; He et al., 2014; Liu et al., 2015; Song et al., 2004). Observations based on  
514 wind-tunnel experiments showed that the NH<sub>3</sub> loss decreased from 14.6 mg L<sup>-1</sup> to 4.5 mg L<sup>-1</sup> as the  
515 depth of floodwater increased from 6.4 cm to 21.3 cm, while other environmental conditions were  
516 similar (Jayaweera et al., 1990). Second, a reduction in the depth of floodwater increases the  
517 volatilization rate constant of NH<sub>3(aq)</sub> ( $k_{vN}$ ), thus increasing NH<sub>3</sub> volatilization from floodwater.  
518 Therefore, compared to the model without floodwater, the modified CNMM-DNDC with the  
519 introduction of a floodwater layer, as well as the corresponding processes, into the simulation of NH<sub>3</sub>  
520 volatilization provided a more scientific algorithm for the simulation of NH<sub>3</sub> loss from rice paddy fields,  
521 thereby enabling the simulation of the pH and NH<sub>4</sub><sup>+</sup> concentration of floodwater. However, the depth of  
522 surface floodwater was kept at a constant value (such as the average depth of the floodwater) for each



523 flooding event in the modified model, but this operation was inconsistent with the field states. The  
524 floodwater depth actually changed with real-time evaporation and precipitation. Therefore, a module  
525 for calculating the dynamics of floodwater depth driven by real-time evaporation and precipitation is  
526 needed to better simulate the effect of floodwater depth on  $\text{NH}_3$  volatilization. The results of this study  
527 suggest that accurate field measurements and a corresponding reliable simulation of floodwater depth  
528 are crucial for the simulation of  $\text{NH}_3$  volatilization by the modified CNMM-DNDC.

#### 529 **4.4 Differences between ammonia volatilization from upland and rice paddy fields**

530 According to the above results, the regulatory factors affecting  $\text{NH}_3$  volatilization from rice paddy  
531 fields were demonstrated to be different from those from cultivated uplands.  $\text{NH}_3$  volatilization from  
532 cultivated uplands was primarily influenced by the regulatory factors of soil properties and field  
533 management practices. However, given the existence of floodwater over rice paddy field soils,  $\text{NH}_3$   
534 volatilization from rice paddy fields was additionally affected by flooding management strategies, such  
535 as floodwater pH and depth. Therefore, the mechanisms and algorithms applied in simulating  $\text{NH}_3$   
536 volatilization from uplands are not appropriate for simulating  $\text{NH}_3$  volatilization from rice paddy fields.  
537 In the modified CNMM-DNDC,  $\text{NH}_3$  volatilization following nitrogen fertilizer application in  
538 cultivated upland soils was based on first-order kinetics. However, the modified CNMM-DNDC  
539 adopted the J-M model, which was based on the two-film theory of mass transfer, to calculate  $\text{NH}_3$   
540 volatilization following nitrogen fertilizer application in rice paddy field soils. The results suggest that  
541 the application of two different mechanisms according to the distinguished properties of cultivated  
542 uplands and rice paddy fields to simulate  $\text{NH}_3$  volatilization is necessary for process-based  
543 biogeochemical models, such as the CNMM-DNDC used in this study.

#### 544 **5. Conclusions**

545 The simulation of ammonia ( $\text{NH}_3$ ) volatilization in the CNMM-DNDC was evaluated and  
546 modified based on 44 and 19 field observation cases of  $\text{NH}_3$  volatilization following synthetic fertilizer  
547 application events in cultivated uplands and rice paddy fields in China, respectively. The original  
548 CNMM-DNDC performed poorly in terms of simulating the observed  $\text{NH}_3$  volatilizations from upland



549 soils, and it failed to simulate  $\text{NH}_3$  volatilization from rice paddy fields because it could not simulate  
550 the water-flooded layer over the rice paddy field. The mechanisms of  $\text{NH}_3$  volatilization from  
551 cultivated uplands and rice paddy fields are different due to the existence of floodwater over rice paddy  
552 soils. Therefore, separate modules simulating  $\text{NH}_3$  volatilization from uplands and rice paddy fields  
553 were developed. The primary modifications for simulating  $\text{NH}_3$  volatilization from upland soils were  
554 mainly adopted from Li et al. (2019), and  $\text{NH}_3$  volatilization from upland soils are regulated by  
555 meteorological conditions, soil properties and crop statuses. In addition, to solve the problem of the  
556 simulation deviation derived from different time steps, a time-step parameter was introduced and  
557 calibrated. With regard to the simulation of  $\text{NH}_3$  volatilization from rice paddy fields, four major  
558 modifications were performed in this study. First, floodwater over rice paddy soil, as well as the  
559 simulation of floodwater pH, was added to the module simulating  $\text{NH}_3$  volatilization from rice paddy  
560 fields. Second, the Jayaweera-Mikkelsen model was newly introduced into the modified  
561 CNMM-DNDC to calculate  $\text{NH}_3$  volatilization from rice paddy fields. Third, the effect of algal growth  
562 on floodwater pH was newly parameterized and added into the model. Finally, the parameters  
563 corresponding to  $\text{NH}_3$  volatilization following ammonium bicarbonate application were calibrated. The  
564 modified model provided an excellent performance in simulating  $\text{NH}_3$  volatilization following  
565 synthetic nitrogen fertilizer applications to either cultivated uplands or rice paddy fields. Nevertheless,  
566 the simulated  $\text{NH}_3$  volatilization following nitrogen fertilizer application by the modified model still  
567 had some deviations from the observations, when deep- or mixed-placement or irrigation/precipitation  
568 were accompanied with the fertilizer event in upland soils and when simulating and limiting factors on  
569 algal growth occurred with fertilizer events in rice paddy fields. A further revision to the modified  
570 model is still needed in future studies to overcome these deficiencies. Nevertheless, the modified  
571 CNMM-DNDC is acceptable for regional or national  $\text{NH}_3$  simulations when developing strategies to  
572 alleviate environmental pollution and compile  $\text{NH}_3$  emission inventories.

573 *Data availability.* All of the model output used to produce the figures can be obtained from the  
574 Supplement, and all of the observed data sets used in this study were collected from published  
575 peer-reviewed articles.



576

577 *Author contribution.* XZ, YL, and WZ contributed to developing the idea and methodology of this  
578 study. SL arranged the research data, improved and implemented the model simulation, prepared the  
579 paper with contributions from all co-authors. RW, KW, and CZ contributed to collect and maintained  
580 the research data. SH, CL, and ZY analyzed study data and verified the results.

581 *Competing interests.* The authors declare that they have no conflict of interest.

582 *Acknowledgments.* This work was supported by the Chinese Academy of Sciences (grant numbers:  
583 ZDBS-LY-DQC007), the National Natural Science Foundation of China (grant numbers: 41907280)  
584 and the China Postdoctoral Science Foundation (grant numbers: 2019M650808).

## 585 **References**

586 Abdalla, M., Song, X., Ju, X., Topp, C. F. E., Smith, P.: Calibration and validation of the DNDC model to  
587 estimate nitrous oxide emissions and crop productivity for a summer maize-winter wheat double  
588 cropping system in Hebei, China, *Environ. Pollut.*, 262, doi:10.1016/j.envpol.2020.114199, 2020.

589 Alberty, R. A.: *Physical chemistry*, John Wiley & Sons, New York, 1983.

590 Anderson, D. M., Burkholder, J. M., Cochlan, W. P., Glibert, P. M., Gobler, C. J., Heil, C. A., Kudela, R.  
591 M., Parsons, M. L., Rensel, J. E. J., Townsend, D. W., Trainer, V. L., Vargo, G. A.: Harmful algal blooms  
592 and eutrophication: Examining linkages from selected coastal regions of the United States, *Harmful*  
593 *Algae*, 8, 39–53, doi:10.1016/j.hal.2008.08.017, 2008.

594 Behera, S. N., Sharma, M., Aneja, V. P., Balasubramanian, R.: Ammonia in the atmosphere: a review on  
595 emission sources, atmospheric chemistry and deposition on terrestrial bodies, *Environ. Sci. Pollut. R.*, 20,  
596 8092–8131, doi:10.1007/s11356-013-2051-9, 2013.

597 Bhagat, R. M., Bhuiyan, S. I., Moody, K.: Water, tillage and weed interactions in lowland tropical rice: a  
598 review, *Agr. Water Manage.*, 31, 165–184, doi:10.1016/0378-3774(96)01242-5, 1996.

599 Bobbink, R., Hornung, M., Roelofs, J. G. M.: The effects of air-borne nitrogen pollutants on species  
600 diversity in natural and semi-natural European vegetation, *J. Ecol.*, 86, 717–738,  
601 doi:10.1046/j.1365-2745.1998.8650717.x, 1998.



- 602 Bouwman, A. F., Lee, D. S., Asman, W. A. H., Dentener, F. J., VanderHoek, K. W., Olivier, J. G. J.: A  
603 global high-resolution emission inventory for ammonia, *Global Biogeochem. Cy.*, 11, 561–587,  
604 doi:10.1029/97gb02266, 1997.
- 605 Bowmer, K. H., Muirhead, W. A.: Inhibition of algal photosynthesis to control pH and reduce ammonia  
606 volatilization from rice floodwater, *Fertil. Res.*, 13, 13–29, doi:10.1007/BF01049799, 1987.
- 607 Buresh, R., Ramesh Reddy, K. and van Kessel, C.: Nitrogen Transformations in Submerged Soils, In:  
608 Raun, J.S.S.a.W.R. editor, *Nitrogen in Agricultural Systems*, 401–436, 2008.
- 609 Cai, G., Peng, G., Wang, X., Zhu, J.: Ammonia volatilization from urea applied to acid paddy soil in  
610 southern china and its control, *Pedosphere*, 2, 345–354, 1992.
- 611 Cai, G., Zhu, Z., Trevitt, A., Freney, J. R., Simpson, J. R.: Nitrogen loss from ammonium bicarbonate  
612 and urea fertilizers applied to flooded rice, *Fertil. Res.*, 10, 203–215, doi:10.1007/BF01049350, 1986.
- 613 Cannavo, P., Recous, S., Parnaudeau, V., Reau, R.: Modeling N dynamics to assess environmental  
614 impacts of cropped soils, *Advances in Agronomy*, 97, Academic Press, 131–174, 2008.
- 615 Cao, Y., Tian, Y., Yin, B., Zhu, Z.: Proliferation of algae and effect of its on fertilizer–N immobilization  
616 in flooded paddy field, *J. Plant Nutr. Fertil. Sc.*, 19, 111–116, doi:10.11674/zwyf.2013.0113, 2013.
- 617 Chien, S. H., Prochnow, L. I., Cantarella, H.: Chapter 8 Recent developments of fertilizer production and  
618 use to improve nutrient efficiency and minimize environmental impacts, *Advances in Agronomy*, 102,  
619 Academic Press, 267–322, 2009.
- 620 De Datta, S. K.: Nitrogen transformations in wetland rice ecosystems, *Fertil. Res.*, 42, 193–203,  
621 doi:10.1007/bf00750514, 1995.
- 622 Duan, Z., Xiao, H.: Effects of soil properties on ammonia volatilization, *Soil Sci. Plant Nutr.*, 46,  
623 845–852, 2000.
- 624 Dubache, G., Li, S., Zheng, X., Zhang, W., Deng, J.: Modeling ammonia volatilization following urea  
625 application to winter cereal fields in the United Kingdom by a revised biogeochemical model, *Sci. Total  
626 Environ.*, 660, 1403–1418, doi:10.1016/j.scitotenv.2018.12.407, 2019.
- 627 Dutta, B., Congreves, K. A., Smith, W. N., Grant, B. B., Rochette, P., Chantigny, M. H., Desjardins, R. L.:  
628 Improving DNDC model to estimate ammonia loss from urea fertilizer application in temperate  
629 agroecosystems, *Nutr. Cycl. Agroecosys.*, 106, 275–292, doi:10.1007/s10705-016-9804-z, 2016.



- 630 Felix, J. D., Elliott, E. M., Gish, T. J., McConnell, L. L., Shaw, S. L.: Characterizing the isotopic  
631 composition of atmospheric ammonia emission sources using passive samplers and a combined  
632 oxidation-bacterial denitrifier approach, *Rapid Commun. Mass Sp.*, 27, 2239–2246,  
633 doi:10.1002/rcm.6679, 2013.
- 634 Fillery, I. R. P., Simpson, J. R., Dedatta, S. K.: Influence of field environment and fertilizer management  
635 on ammonia loss from flooded rice, *Soil Sci. Soc. Am. J.*, 48, 914–920,  
636 doi:10.2136/sssaj1984.03615995004800040043x, 1984.
- 637 Fillery, I. R. P., Vlek, P. L. G.: 4. Reappraisal of the significance of ammonia volatilization as an N loss  
638 mechanism in flooded rice fields, *Fertil. Res.*, 9, 79–98, doi:10.1007/BF01048696, 1986.
- 639 Freney, J. R., Simpson, J. R.: Gaseous loss of nitrogen from plant-soil systems, *Developments in plant  
640 and soil sciences*, 9, 1983.
- 641 Freney, J. R., Trevitt, A. C. F., Muirhead, W. A., Denmead, O. T., Simpson, J. R., Obcemea, W. N.: Effect  
642 of water depth on ammonia loss from lowland rice, *Fertil. Res.*, 16, 97–107, doi:10.1007/bf01049767,  
643 1988.
- 644 Giltrap, D., Saggarr, S., Rodriguez, J., Bishop, P.: Modelling NH<sub>3</sub> volatilisation within a urine patch using  
645 NZ-DNDC, *Nutr. Cycl. Agroecosys.*, 108, 267–277, doi:10.1007/s10705-017-9854-x, 2017.
- 646 Gong, W., Zhang, Y., Huang, X., Luan, S.: High-resolution measurement of ammonia emissions from  
647 fertilization of vegetable and rice crops in the Pearl River Delta Region, China, *Atmos. Environ.*, 65,  
648 1–10, doi:10.1016/j.atmosenv.2012.08.027, 2013.
- 649 Han, K., Zhou, C., Wang, L.: Reducing ammonia volatilization from maize fields with separation of  
650 nitrogen fertilizer and water in an alternating furrow irrigation system, *J. Integr. Agr.*, 13, 1099–1112,  
651 doi:10.1016/s2095-3119(13)60493-1, 2014.
- 652 Hayashi, K., Nishimura, S., Yagi, K.: Ammonia volatilization from the surface of a Japanese paddy field  
653 during rice cultivation, *Soil Sci. Plant Nutr.*, 52, 545–555, doi:10.1111/j.1747-0765.2006.00053.x, 2006.
- 654 He, Y., Yang, S., Xu, J., Wang, Y., Peng, S.: Ammonia volatilization losses from paddy fields under  
655 controlled irrigation with different drainage treatments, *Sci. World J.*, doi:10.1155/2014/417605, 2014.
- 656 Holcomb III, J. C., Sullivan, D. M., Horneck, D. A., Clough, G. H.: Effect of irrigation rate on ammonia  
657 volatilization, *Soil Sci. Soc. Am. J.*, 75, 2341–2347, doi:10.2136/sssaj2010.0446, 2011.



- 658 Huang, X., Song, Y., Li, M., Li, J., Huo, Q., Cai, X., Zhu, T., Hu, M., Zhang, H.: A high-resolution  
659 ammonia emission inventory in China, *Global Biogeochem. Cy.*, 26, GB1030,  
660 doi:10.1029/2011gb004161, 2012.
- 661 Jayaweera, G. R., Mikkelsen, D. S.: Ammonia volatilization from flooded soil systems - a  
662 computer-model. I. Theoretical aspects, *Soil Sci. Soc. Am. J.*, 54, 1447–1455,  
663 doi:10.2136/sssaj1990.03615995005400050039x, 1990a.
- 664 Jayaweera, G. R., Mikkelsen, D. S.: Ammonia volatilization from flooded soil systems - a  
665 computer-model. II. Theory and model results, *Soil Sci. Soc. Am. J.*, 54, 1456–1462,  
666 doi:10.2136/sssaj1990.03615995005400050040x, 1990b.
- 667 Jayaweera, G. R., Mikkelsen, D. S.: Assessment of ammonia volatilization from flooded soil systems,  
668 *Adv. Agron.*, 45, 303–356, doi:10.1016/S0065-2113(08)60044-9, 1991.
- 669 Jayaweera, G. R., Paw U., K. T., Mikkelsen, D. S.: Ammonia volatilization from flooded soil systems: a  
670 computer model. III. Validation of the model, *Soil Sci. Soc. Am. J.*, 54, 1462–1468,  
671 doi:10.2136/sssaj1990.03615995005400050041x, 1990.
- 672 Kong, L., Tang, X., Zhu, J., Wang, Z., Pan, Y., Wu, H., Wu, L., Wu, Q., He, Y., Tian, S., Xie, Y., Liu, Z.,  
673 Sui, W., Han, L., Carmichael, G.: Improved inversion of monthly ammonia emissions in China based on  
674 the Chinese ammonia monitoring network and ensemble Kalman filter, *Environ. Sci. Technol.*, 53,  
675 12529–12538, doi:10.1021/acsest.9b02701, 2019.
- 676 Lei, T., Guo, X., Ma, J., Sun, X., Feng, Y., Wang, H.: Kinetic and thermodynamic effects of moisture  
677 content and temperature on the ammonia volatilization of soil fertilized with urea, *Int. J. Agr. Biol. Eng.*,  
678 10, 134–143, doi:10.25165/j.ijabe.20171006.3232, 2017.
- 679 Li, C.: *Biogeochemistry: Scientific fundamentals and modelling approach*, Tsinghua University Press,  
680 Beijing, 2016.
- 681 Li, C., Frolking, S., Frolking, T. A.: A model of nitrous-oxide evolution from soil driven by rainfall  
682 events. 1. Model structure and sensitivity, *J. Geophys. Res. - Atmos.*, 97, 9759–9776,  
683 doi:10.1029/92jd00509, 1992.
- 684 Li, H., Han, Y., Cai, Z.: Modeling the ammonia volatilization from common urea and controlled releasing  
685 urea fertilizers in paddy soil of Taihu region of China by Jayaweera–Mikkelsen model, *Environ. Sci.*, 29,



- 686 1045–1052, doi:10.1007/BF01049507, 2008.
- 687 Li, S., Zheng, X., Zhang, W., Han, S., Deng, J., Wang, K., Wang, R., Yao, Z., Liu, C.: Modeling ammonia  
688 volatilization following the application of synthetic fertilizers to cultivated uplands with calcareous soils  
689 using an improved DNDC biogeochemistry model, *Sci. Total Environ.*, 660, 931–946,  
690 doi:10.1016/j.scitotenv.2018.12.379, 2019.
- 691 Li, Y., Schichtel, B. A., Walker, J. T., Schwede, D. B., Chen, X., Lehmann, C. M. B., Puchalski, M. A.,  
692 Gay, D. A., Collett, J. L., Jr.: Increasing importance of deposition of reduced nitrogen in the United States,  
693 *P. Nat. Acad. Sci., USA* 113, 5874–5879, doi:10.1073/pnas.1525736113, 2016.
- 694 Li, Y., Shen, J., Wang, Y., Gao, M., Liu, F., Zhou, P., Liu, X., Chen, D., Zou, G., Luo, Q., Ma, Q.: CNMM:  
695 a grid-based spatially-distributed catchment simulation model, China Science Press, Beijing, 2017.
- 696 Liu, J., Ding, P., Zong, Z., Li, J., Tian, C., Chen, W., Chang, M., Salazar, G., Shen, C., Cheng, Z., Chen,  
697 Y., Wang, X., Szidat, S., Zhang, G.: Evidence of rural and suburban sources of urban haze formation in  
698 China: a case study from the Pearl River Delta region, *J. Geophys. Res. - Atmos.*, 123, 4712–4726,  
699 doi:10.1029/2017jd027952, 2018.
- 700 Liu, T., Fan, D., Zhang, X., Chen, J., Li, C., Cao, C.: Deep placement of nitrogen fertilizers reduces  
701 ammonia volatilization and increases nitrogen utilization efficiency in no-tillage paddy fields in central  
702 China, *Field Crops Res.*, 184, 80–90, doi:10.1016/j.fcr.2015.09.011, 2015.
- 703 Liu, X., Ju, X., Zhang, F., Pan, J., Christie, P.: Nitrogen dynamics and budgets in a winter wheat–maize  
704 cropping system in the North China Plain, *Field Crops Res.*, 83, 111–124,  
705 doi:10.1016/S0378-4290(03)00068-6, 2003.
- 706 Mariano, E., de Sant Ana Filho, C. R., Bortoletto-Santos, R., Bendassolli, J. A., Trivelin, P. C. O.:  
707 Ammonia losses following surface application of enhanced-efficiency nitrogen fertilizers and urea,  
708 *Atmos. Environ.*, 203, 242–251, doi:10.1016/j.atmosenv.2019.02.003, 2019.
- 709 Martens, D. A., Bremner, J. M.: Soil properties affecting volatilization of ammonia from soils treated  
710 with urea, *Commun. Soil Sci. Plan.*, 20, 1645–1657, doi:10.1080/00103628909368173, 1989.
- 711 Martin, S. T., Hung, H. M., Park, R. J., Jacob, D. J., Spurr, R. J. D., Chance, K. V., Chin, M.: Effects of  
712 the physical state of tropospheric ammonium-sulfate-nitrate particles on global aerosol direct radiative  
713 forcing, *Atmos. Chem. Phys.*, 4, 183–214, doi:10.5194/acp-4-183-2004, 2004.



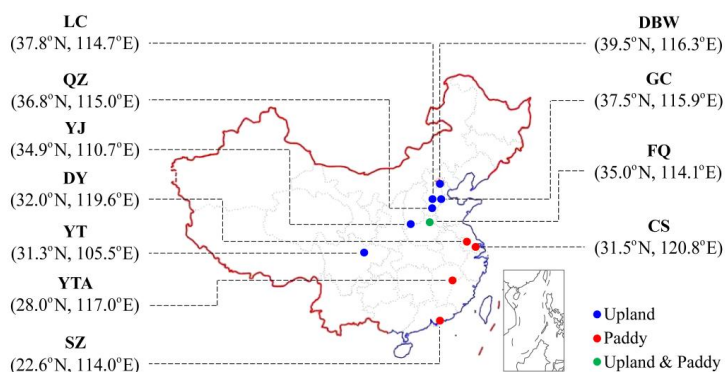
- 714 Michalczyk, A., Kersebaum, K.C., Heimann, L., Roelcke, M., Sun, Q. P., Chen, X. P., Zhang, F. S.:  
715 Simulating in situ ammonia volatilization losses in the North China Plain using a dynamic soil-crop  
716 model, *J. Plant Nutr. Soil Sc.*, 179, 270–285, doi:10.1002/jpln.201400673, 2016.
- 717 Mikkelsen, D. S., Datta, S. K. D., Obcemea, W. N.: Ammonia volatilization losses from flooded rice  
718 soils, *Soil Sci. Soc. Am. J.*, 42, 725–730, doi:10.2136/sssaj1978.03615995004200050043x, 1978.
- 719 Park, K. D., Lee, D. W., Li, Y., Chen, D., Park, C. Y., Lee, Y. H., Lee, C. H., Kang, U. G., Park, S. T., Cho,  
720 Y. S.: Simulating ammonia volatilization from applications of different urea applied in rice field by  
721 WNMM, *Korean J. Crop Sci.*, 53, 8–14, 2008.
- 722 Paulot, F., Jacob, D. J., Pinder, R. W., Bash, J. O., Travis, K., Henze, D. K.: Ammonia emissions in the  
723 United States, European Union, and China derived by high-resolution inversion of ammonium wet  
724 deposition data: Interpretation with a new agricultural emissions inventory (MASAGE\_NH<sub>3</sub>), *J.*  
725 *Geophys. Res. - Atmos.*, 119, 4343–4364, doi:10.1002/2013jd021130, 2014.
- 726 Riddick, S., Ward, D., Hess, P., Mahowald, N., Massad, R., Holland, E.: Estimate of changes in  
727 agricultural terrestrial nitrogen pathways and ammonia emissions from 1850 to present in the  
728 Community Earth System Model, *Biogeosciences*, 13, 3397–3426, doi:10.5194/bg-13-3397-2016, 2016.
- 729 Roelcke, M., Li, S., Tian, X., Gao, Y., Richter, J.: In situ comparisons of ammonia volatilization from N  
730 fertilizers in Chinese loess soils, *Nutr. Cycl. Agroecosys.*, 62, 73–88, doi:10.1023/a:1015186605419,  
731 2002.
- 732 Sanz-Cobena, A., Misselbrook, T., Camp, V., Vallejo, A.: Effect of water addition and the urease  
733 inhibitor NBPT on the abatement of ammonia emission from surface applied urea, *Atmos. Environ.*, 45,  
734 1517–1524, doi:10.1016/j.atmosenv.2010.12.051, 2011.
- 735 Savard, M. M., Cole, A., Smirnov, A., Vet, R.:  $\delta^{15}\text{N}$  values of atmospheric N species simultaneously  
736 collected using sector - based samplers distant from sources isotopic inheritance and fractionation,  
737 *Atmos. Environ.*, 162, 11–22, doi:10.1016/j.atmosenv.2017.05.010, 2017.
- 738 Schjørring, J. K.: Atmospheric ammonia and impacts of nitrogen deposition: Uncertainties and  
739 challenges, *New Phytol.*, 139, 59–60, doi:10.1046/j.1469-8137.1998.00173.x, 1998.
- 740 Sommer, S. G., Schjoerring, J. K., Denmead, O. T.: Ammonia emission from mineral fertilizers and  
741 fertilized crops, In: Sparks, D.L. editor, *Advances in Agronomy*, 82, 557–622, 2004.



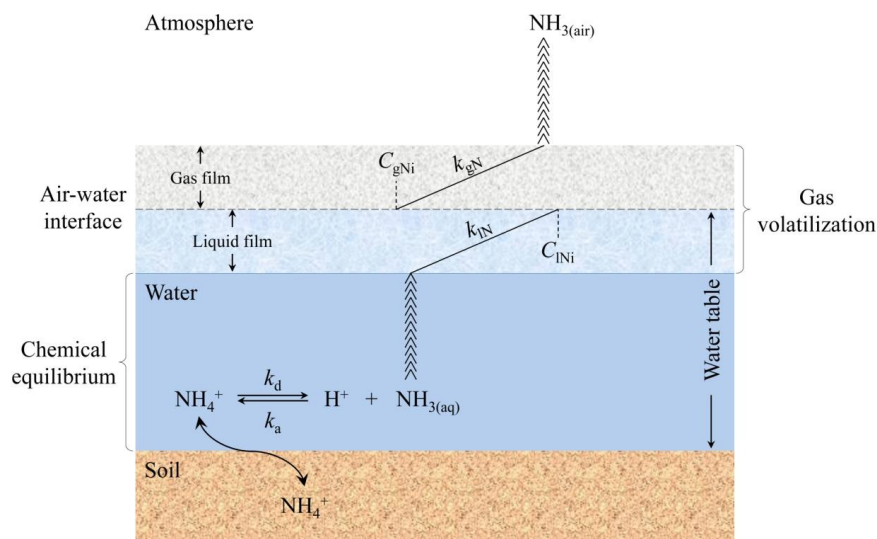
- 742 Song, Y., Fan, X., Lin, D., Yang, L., Zhou, J.: Ammonia volatilization from paddy fields in the Taihu lake  
743 region and its influencing factors, *Acta Pedologica Sinica*, 265–269, doi:10.11766/trxb200306090216,  
744 2004.
- 745 Wang, H., Hu, Z., Lu, J., Liu, X., Wen, G., Blaylock, A.: Estimation of ammonia volatilization from a  
746 paddy field after application of controlled-release urea based on the modified Jayaweera-Mikkelsen  
747 model combined with the Sherlock-Goh model, *Commun. Soil Sci. Plan.*, 47, 1630–1643,  
748 doi:10.1080/00103624.2016.1206120, 2016.
- 749 Xu, R., Tian, H., Pan, S., Prior, S. A., Feng, Y., Batchelor, W. D., Chen, J., Yang, J.: Global ammonia  
750 emissions from synthetic nitrogen fertilizer applications in agricultural systems: Empirical and  
751 process-based estimates and uncertainty, *Global Change Biol.*, 25, 314–326, doi:10.1111/gcb.14499,  
752 2019.
- 753 Zhan, X., Chen, C., Wang, Q., Zhou, F., Hayashi, K., Ju, X., Lam, S. K., Wang, Y., Wu, Y., Fu, J., Zhang,  
754 L., Gao, S., Hou, X., Bo, Y., Zhang, D., Liu, K., Wu, Q., Su, R., Zhu, J., Yang, C., Dai, C., Liu, H.:  
755 Improved Jayaweera-Mikkelsen model to quantify ammonia volatilization from rice paddy fields in  
756 China, *Environ. Sci. Pollut. R.*, 26, 8136–8147, doi:10.1007/s11356-019-04275-2, 2019.
- 757 Zhang, S., Cai, G., Wang, X., Xu, Y., Zhu, Z., Freney, J. R.: Losses of urea-nitrogen applied to maize  
758 grown on a calcareous Fluvo-Aquic soil in North China Plain, *Pedosphere*, 171–178,  
759 doi:10.1109/34.142909, 1992.
- 760 Zhang, W., Li, S., Han, S., Xie, H., Lu, C., Sui, Y., Rui, W., Liu, C., Yao, Z., Zheng, X.: Less intensive  
761 nitrate leaching from Phaeozems cultivated with maize generally occurs in northeastern China, *Agr.*  
762 *Ecosyst. Environ.*, doi:10.1016/j.agee.2021.107303, 2021.
- 763 Zhang, W., Li, Y., Zhu, B., Zheng, X., Liu, C., Tang, J., Su, F., Zhang, C., Ju, X., Deng, J.: A  
764 process-oriented hydro-biogeochemical model enabling simulation of gaseous carbon and nitrogen  
765 emissions and hydrologic nitrogen losses from a subtropical catchment, *Sci. Total Environ.*, 616,  
766 305–317, doi:10.1016/j.scitotenv.2017.09.261, 2018.
- 767 Zhang, W., Yao, Z., Zheng, X., Liu, C., Rui, W., Wang, K., Li, S., Han, S., Zuo, Q., Shi, J.: Effects of  
768 fertilization and stand age on N<sub>2</sub>O and NO emissions from tea plantations: a site-scale study in a  
769 subtropical region using a modified biogeochemical model, *Atmos. Chem. Phys.*, 20, 6903–6919,



770 doi:10.5194/acp-20-6903-2020, 2020.  
771 Zhou, F., Ciais, P., Hayashi, K., Galloway, J., Kim, D. G., Yang, C., Li, S., Liu, B., Shang, Z., Gao, S.:  
772 Re-estimating NH<sub>3</sub> emissions from Chinese cropland by a new nonlinear model, Environ. Sci. Technol.,  
773 50, 564–572, doi:10.1021/acs.est.5b03156, 2016.  
774 Zhu, Z., Cai, G., Simpson, J. R., Zhang, S., Chen, D., Jackson, A. V., Freney, J. R.: Processes of nitrogen  
775 loss from fertilizers applied to flooded rice fields on a calcareous soil in north–central China, Nutr. Cycl.  
776 Agroecosys., 18, 101–115, doi:10.1007/BF01049507, 1989.  
777



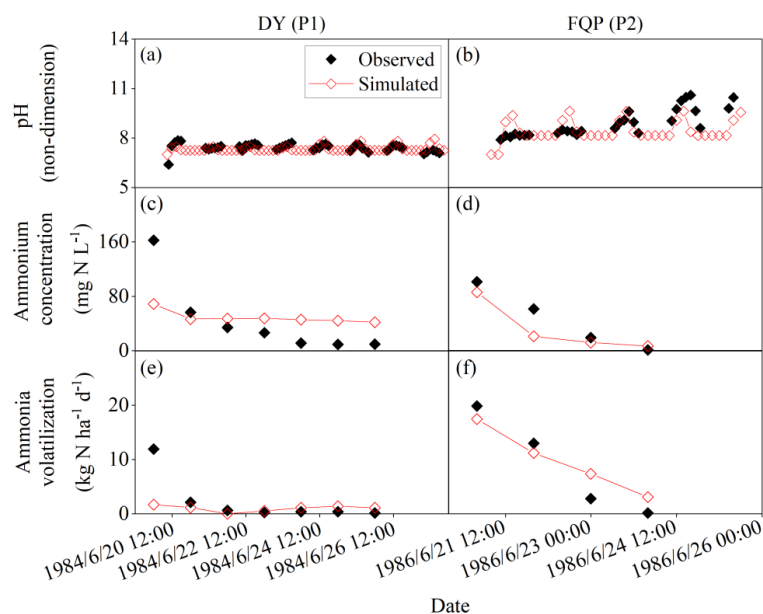
778  
779 **Fig. 1** Location of the experimental field sites involved in this study. The sites are Changshu (CS),  
780 Danyang (DY), Dongbeiwang (DBW), Fengqiu (FQ), Guangchuan (GC), Luancheng (LC),  
781 Quzhou (QZ), Shenzhen (SZ), Yanting (YT), Yingtan (YTA), and Yongji (YJ).  
782



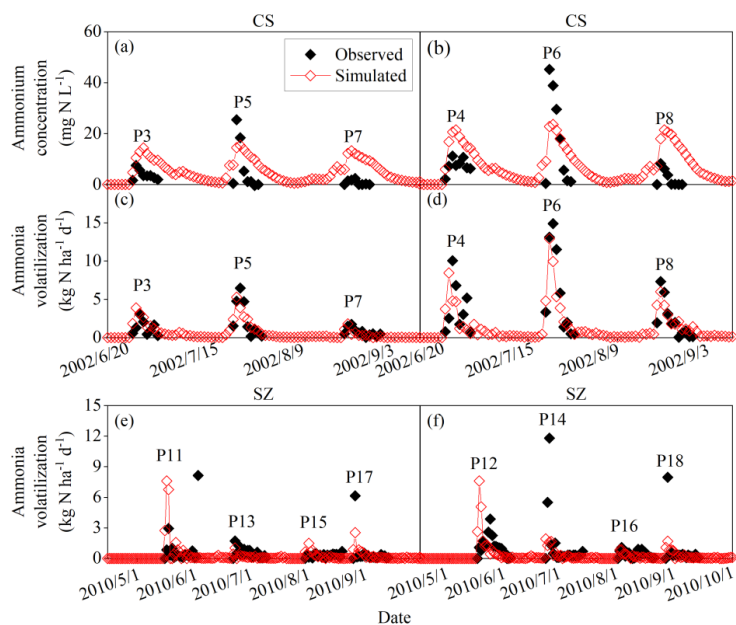
783

784 **Fig. 2 Mechanism of the Jayaweera-Mikkelsen model introduced into the modified CNMM-DNDC.**  
 785  $k_d$  and  $k_a$  are referred to as the dissociation and association rate constants for  $\text{NH}_4^+/\text{NH}_3$  chemical  
 786 equilibrium, respectively.  $k_{IN}$  and  $k_{gN}$  are referred to as the exchange constants for  $\text{NH}_3$  in the  
 787 liquid and gas films, respectively.  $C_{INI}$  and  $C_{gNi}$  are referred to as the average concentrations of  $\text{NH}_3$   
 788 at the interface in the liquid and gas films, respectively.  $\text{NH}_{3(\text{aq})}$  and  $\text{NH}_{3(\text{air})}$  are referred to as the  
 789 average concentration of  $\text{NH}_3$  in aqueous and gas phases, respectively.

790



791  
792 **Fig. 3** Observed and simulated pH and ammonium concentrations of floodwater and daily  
793 ammonia volatilization from the ammonium carbonate application for DY and FQP. The  
794 definitions of the case codes are referred to Table 2. The sites are Danyang (DY) and Fengjiu  
795 with rice paddy fields (FQP).  
796



797

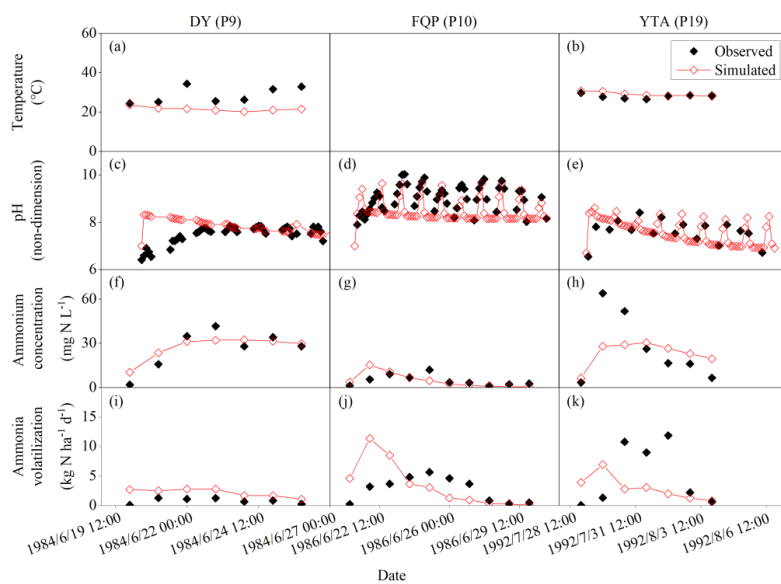
798

799

800

801

**Fig. 4** Observed and simulated ammonium concentrations of floodwater and daily ammonia volatilization from the urea application for CS and SZ. The definitions of the case codes are referred to Table 2. The sites are Changshu (CS) and Shenzhen (SZ).

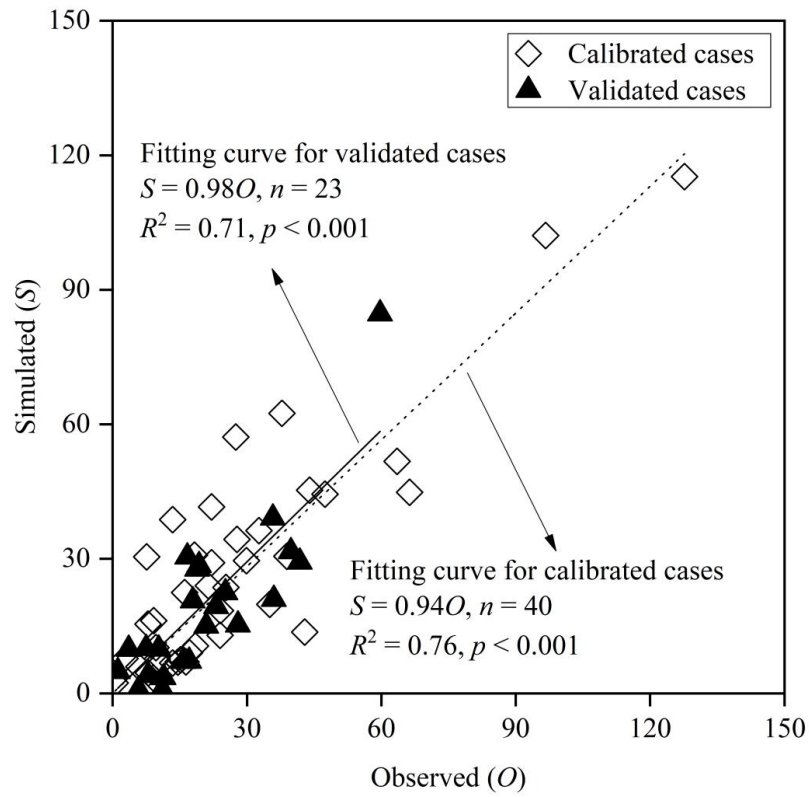


802

803 **Fig. 5** Observed and simulated temperatures, pH and ammonium concentrations of floodwater  
804 and daily ammonia volatilization from the urea application for DY, FQP and YTA. The definitions  
805 of the case codes are referred to Table 2. The sites are Danyang (DY), Fengqiu with rice paddy  
806 fields (FQP) and Yingtan (YTA).

807

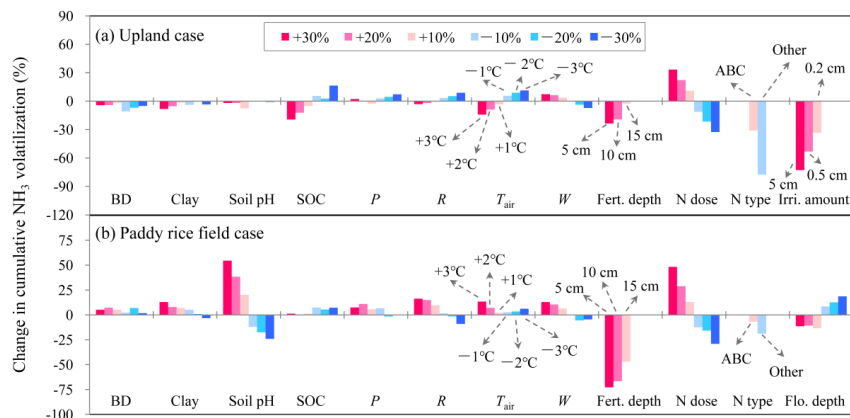
808



809

810 **Fig. 6** Comparison between the observed and simulated cumulative ammonia volatilization across  
811 all calibrated and validated cases of upland and rice paddy fields.  $n$ ,  $p$  and  $R^2$  denote the sample  
812 size, significance level and coefficient of determination for the zero-intercept linear regression,  
813 respectively.

814



815

816 **Fig. 7** Sensitivity analysis of the modified CNMM-DNDC in simulating cumulative ammonia ( $\text{NH}_3$ )  
 817 volatilization from uplands and rice paddy fields during the measurement periods through change  
 818 input factors. The investigated input factors include: 3-hourly averages of air temperature ( $T_{\text{air}}$ )  
 819 and wind speed ( $W$ ); 3-hourly totals of precipitation ( $P$ ) and solar radiation ( $R$ ) during individual  
 820 measurement periods of  $\text{NH}_3$  volatilization; soil clay fraction, pH, organic carbon (SOC) content  
 821 and bulk density (BD); irrigation water amount (Irri. amount) and floodwater depth (Flo. depth);  
 822 and, nitrogen fertilization depth, dose and type (Fert. depth, N dose, and N type, respectively). The  
 823 N types include ammonium bicarbonate (ABC) and other ammonium-based nitrogen fertilizers  
 824 (Other). The legends within the frame apply to all the subfigures and all the factors without notes  
 825 highlighted by arrows.

826



827 **Table 1** Descriptive information of the studied experimental sites of rice paddy fields for model  
828 evaluation, including site name, experimental year (Year), crop rotation (Crop), fertilizer type (Type)  
829 and dose (Dose, kg N ha<sup>-1</sup>), measurement method for ammonia volatilization (Method), number of  
830 fertilization cases (Number) and reference (Ref.).

Site <sup>a</sup>	Year	Crop <sup>b</sup>	Type	Dose	Method <sup>d</sup>	Number	Ref. <sup>e</sup>
CS	2002–2003	RW	Urea	41–135	MM	6	[1]
DY	1984	RW	Urea/ABC <sup>c</sup>	90	MM	2	[2]
FQP	1986	RW	Urea/ABC	90	MM	2	[3]
SZ	2010	DR	Urea	41–162	WT	8	[4]
YTA	1992	DR	Urea	90	MM	1	[5]

831 <sup>a</sup> The sites are Changshu (CS), Danyang (DY), Fengqiu with rice paddy fields (FQP), Shenzhen (SZ),  
832 and Yingtan (YTA).

833 <sup>b</sup> The presented crop rotation types are rice–wheat (RW) and double rice (DR).

834 <sup>c</sup> ABC is the abbreviation of ammonium bicarbonate.

835 <sup>d</sup> The presented methods for the measurement of ammonia volatilization are wind tunnel (WT) and  
836 micrometeorological technique (MM).

837 <sup>e</sup> [1] Song et al., 2004; [2] Cai et al., 1986; [3] Zhu et al., 1989; [4] Gong et al., 2013; and [5] Cai et al.,  
838 1992.



840 **Table 2** Observed and simulated cumulative ammonia volatilization during the measurement periods,  
 model biases, and management practices of individual fertilizer application cases in the rice paddy  
 fields.

Case code <sup>a</sup>	Site <sup>b</sup>	Period	$O^c$	$S^c$	RMB <sup>c</sup>	Water table <sup>d</sup>	Pre <sup>e</sup>	Fertilizer application		
								Type <sup>f</sup>	Method <sup>g</sup>	Dose <sup>h</sup>
P1 <sup>@</sup>	DY	Jun. 20 to Jun. 26, 1984	16.4	7.04	-57.0	5	0	ABC	BFT5	90
P2	FQP	Jun. 21 to Jun. 30, 1986	35.8	39.13	9.3	4	0.18	ABC	BFT5	90
P3	CS	Jun. 22 to Jun. 30, 2002	10.3	9.89	-4.0	4 <sup>*</sup>	6.38	Urea	B	40.5
P4	CS	Jun. 22 to Jun. 30, 2002	23.1	19.40	-16.0	4 <sup>*</sup>	6.38	Urea	B	81
P5	CS	Jul. 20 to Jul. 29, 2002	20.9	15.04	-28.0	4 <sup>*</sup>	0.54	Urea	B	54
P6	CS	Jul. 20 to Jul. 29, 2002	39.8	31.61	-20.6	4 <sup>*</sup>	0.54	Urea	B	108
P7	CS	Aug. 20 to Aug. 31, 2002	7.5	10.02	33.6	4 <sup>*</sup>	3.07	Urea	B	40.5
P8	CS	Aug. 20 to Aug. 31, 2002	17.9	20.68	15.5	4 <sup>*</sup>	3.07	Urea	B	81
P9 <sup>@</sup>	DY	Jun. 20 to Jun. 26, 1984	7.9	15.44	94.9	5	0	Urea	BFT5	90
P10 <sup>@</sup>	FQP	Jun. 21 to Jun. 30, 1986	27.8	34.32	23.7	4	0.18	Urea	BFT5	90
P11 <sup>@</sup>	SZ	May 16 to Jun. 4, 2010	16.1	22.50	39.8	7.5 <sup>#</sup>	0	Urea	B	162.2
P12 <sup>@</sup>	SZ	May 16 to Jun. 4, 2010	21.4	24.00	12.2	7.5 <sup>#</sup>	0	Urea	B	162.2
P13 <sup>@</sup>	SZ	Jun. 22 to Jul. 11, 2010	9.1	3.43	-62.4	7.5 <sup>#</sup>	0	Urea	B	40.9
P14 <sup>@</sup>	SZ	Jun. 22 to Jul. 11, 2010	17.2	9.07	-47.3	7.5 <sup>#</sup>	0	Urea	B	81.8
P15 <sup>@</sup>	SZ	Jul. 31 to Aug. 19, 2010	5.9	5.92	0.3	7.5 <sup>#</sup>	0	Urea	B	40.9
P16 <sup>@</sup>	SZ	Jul. 31 to Aug. 19, 2010	8.0	4.57	-42.9	7.5 <sup>#</sup>	0	Urea	B	40.9
P17 <sup>@</sup>	SZ	Aug. 26 to Sep. 14, 2010	10.0	7.66	-23.4	7.5 <sup>#</sup>	0	Urea	B	81.8
P18 <sup>@</sup>	SZ	Aug. 26 to Sep. 14, 2010	13.4	6.79	-49.3	7.5 <sup>#</sup>	0	Urea	B	81.8
P19	YTA	Jul. 29 to Aug. 6, 1992	36.0	20.98	-41.7	2	1.36	Urea	BFT5	90

<sup>a</sup> P1 to P19 encode the experimental cases following individual application events of synthetic nitrogen fertilizers; the superscript “@” symbol marks the cases with the ammonia observations being referred to the model calibration.

845 <sup>b</sup> The sites are Changshu (CS), Danyang (DY), Fengqiu with rice paddy fields (FQP), Shenzhen (SZ), and Yingtan (YTA).

<sup>c</sup>  $O$  and  $S$  are the cumulative  $\text{NH}_3$  volatilization ( $\text{kg N ha}^{-1}$ ) observed and simulated by the modified CNMM-DNDC, respectively; RMB is the relative model bias (%) of the modified model, each of which was determined as the relative difference between the simulated and observed values.

850 <sup>d</sup> The depth of floodwater table (cm). For the cases with “\*” and “#”, the exact depth of the floodwater table was not reported. The floodwater table depth of the cases with “\*” was arbitrarily set as the traditional depth of the floodwater table of the DY site, which was located in the same region. The floodwater depths of the cases with “#” were set by model calibration.

<sup>e</sup> Pre denotes total rainfall (cm) during the experimental period(s).

855 <sup>f</sup> ABC is the fertilizer type of ammonium bicarbonate.

<sup>g</sup> The application methods are surface broadcast (B) and broadcast followed by tillage (BFT). The figures following BFT are the depth in soil (cm).

<sup>h</sup> Unit:  $\text{kg N ha}^{-1}$ .



**Table 3** Statistical indices for evaluating the performance of the modified CNMM-DNDC in simulating daily and cumulative ammonia ( $\text{NH}_3$ ) fluxes from ammonium bicarbonate (ABC) and urea (including other fertilizer types) applications for the independent calibration (Cal) and validation (Val) cases in uplands and rice paddy fields.

Land use	$\text{NH}_3$ flux	Fertilizer type	Operation	Num	IA	NSI	ZIR		
							Slope	$R^2$	$p$
Upland	Daily	ABC	Cal	39	0.5	-1.34	0.53	na	na
			Val	24	0.60	-0.51	0.69	na	na
		Urea	Cal	287	0.44	-0.06	0.38	na	na
			Val	137	0.67	0.02	0.64	0.09	< 0.001
	Cumulative	ABC	Cal	3	0.75	0.14	0.73	0.64	ns
			Val	2	-	-	-	-	-
		Urea	Cal	26	0.93	0.73	0.94	0.71	< 0.001
			Val	13	0.91	0.49	1.06	0.74	< 0.001
Rice paddy field	Daily	ABC	Cal	7	0.33	0.02	0.16	na	na
			Val	4	0.94	0.85	0.90	0.71	ns
		Urea	Cal	176	0.53	-0.35	0.47	0.04	< 0.05
			Val	63	0.72	0.36	0.56	0.19	< 0.001
	Cumulative	ABC	Cal	1	-	-	-	-	-
			Val	1	-	-	-	-	-
		Urea	Cal	10	0.88	0.30	1.03	0.68	< 0.01
			Val	7	0.85	0.60	0.77	0.65	< 0.05

The statistical indices are the index of agreement (IA), Nash–Sutcliffe Index (NSI), and the slope, determination coefficient ( $R^2$ ) and significance level ( $p$ ) of the zero-intercept univariate linear regression (ZIR) of observations against simulations. Being not available (na) indicates a negative  $R^2$  and a suffering  $F$ -test. Being not significant (ns) indicates a ZIR with  $p > 0.05$ . Num is the abbreviation of sample number.



870 **Table 4** Statistical indices for evaluating the performance of the CNMM-DNDC in simulating the daily temperature ( $T$ ), pH and ammonium concentration ( $\text{NH}_4^+$ ) in floodwater for the calibration (Cal) and validation (Val) cases.

Variables	Operation	Num	Cases	IA	NSI	ZIR		
						Slope	$R^2$	$p$
$T$	Cal	7	P9	0.43	-3.50	1.32	na	na
	Val	7	P19	0.51	-1.76	0.96	na	na
pH	Cal	147	P1, P9, P10	0.83	0.55	1.00	0.55	< 0.001
	Val	45	P2, P19	0.79	0.36	1.01	0.36	< 0.001
$\text{NH}_4^+$	Cal	24	P1, P9, P10	0.78	0.48	1.03	0.48	< 0.001
	Val	55	P2, P3–P8	0.68	0.25	0.74	0.34	< 0.001

875 The statistical indices are the index of agreement (IA), Nash–Sutcliffe Index (NSI), and the slope, determination coefficient ( $R^2$ ) and significance level ( $p$ ) of the zero-intercept univariate linear regression (ZIR) of observations against simulations. Being not available (na) indicates a negative  $R^2$  and a suffering  $F$ -test. Being not significant (ns) indicates a ZIR with  $p > 0.05$ . Num is the abbreviation of sample number. The definitions of the case codes are referred to Table 2.